Impacts of *APOE-ε4* and exercise training on brain microvascular endothelial cell barrier function and metabolism

Callie M. Weber,[a] Bilal Moiz,[a] Gabriel S. Pena,[b] Marzyeh Kheradmand,[a] Brooke Wunderler,[a] Claire Kettula,[a] Gurneet S. Sangha,[a] J. Carson Smith,[b] and Alisa Morss Clyne[a,*]

[a]Department of Bioengineering, University of Maryland; College Park, MD, 20742, United States
[b]Department of Kinesiology, University of Maryland, College Park, MD, 20742, United States

eBioMedicine
2025;111: 105487
Published Online xxx
https://doi.org/10.1016/j.ebiom.2024.105487

Summary

Background The *APOE-ε4* genotype is the highest genetic risk factor for Alzheimer's disease (AD), and exercise training can reduce the risk of AD. Two early pathologies of AD are degradation of tight junctions between brain microvascular endothelial cells (BMEC) and brain glucose hypometabolism. Therefore, the objective of this work was to determine how the *APOE-ε4* genotype and serum from exercise trained individuals impacts BMEC barrier function and metabolism.

Methods iPSC homozygous for the *APOE-ε3* and *APOE-ε4* alleles were differentiated to BMEC-like cells and used to measure barrier function and metabolism. To investigate exercise effects, serum was collected from older adults pre- and post- 6 months of exercise training (n = 9 participants per genotype). *APOE-ε3* and *APOE-ε4* BMEC were treated with genotype-matched serum, and then barrier function and metabolism were measured.

Findings *APOE-ε4* genotype impaired BMEC barrier function and metabolism by reducing sirtuin 1 (SIRT1) levels by 27% (p = 0.0188) and baseline insulin signalling by 37% (p = 0.0186) compared to *APOE-ε3* BMEC. Exercise-trained serum increased SIRT1 by 33% (p = 0.0043) in *APOE-ε3* BMEC but decreased SIRT1 by 22% (p = 0.0004) in *APOE ε4* BMEC.

Interpretation *APOE-ε4* directly impairs glucose metabolism and barrier function. Serum from exercise trained individuals alters SIRT1 in a genotype-dependent manner but may require additional cues from exercise to decrease AD pathologies.

Funding Brain and Behaviour Initiative at the University of Maryland through the Seed Grant Program, NSF-GRFP DGE 1840340, Fischell Fellowship in Biomedical Engineering, NSF CBET-2211966 and DGE-1632976, National Niemann-Pick Disease Foundation, University of Maryland ASPIRE Program, NIH R01HL165193, R01HL140239-01, and R01AG057552.

Keywords: Blood-brain barrier; Alzheimer's disease; Glucose metabolism; APOE genotype; Exercise training

Introduction

The *APOE-ε4* genotype is the strongest genetic risk factor for AD and also increases the risk of vascular disease.[1] Individuals homozygous for the *APOE-ε4* allele have a ten-fold higher risk for AD and develop clinically detectable AD manifestations 7–10 years before individuals homozygous for the *APOE-ε3* allele.[2,3] Even so, not all *APOE-ε4* allele carriers develop AD, suggesting vulnerability to AD may be modifiable through lifestyle behaviours. Consistent exercise training is estimated to reduce AD risk by 45%,[4] though it is unknown if individuals with the *APOE-ε3* and *-ε4* genotypes receive equal benefit from exercise training.

Brain microvascular endothelial cells (BMEC) line the cerebral blood vessels and have specialised tight junctions designed to strictly regulate nutrient and waste transfer between the blood and the brain. Two early indicators of AD development are breakdown of the tight junctions and whole brain glucose hypometabolism. In humans, the *APOE-ε4* genotype is correlated with many AD biomarkers, including increased blood–brain barrier (BBB) permeability,[5] decreased brain glucose metabolism,[6] and increased amyloid-β (Aβ) and tau accumulation.[7] In mice, the *APOE-ε4* genotype reduced BMEC barrier function[8–10] and glycolysis[9] compared to the *APOE-ε3* genotype.

*Corresponding author.
E-mail address: aclyne@umd.edu (A.M. Clyne).

Research in context

Evidence before this study

We reviewed the literature using traditional (e.g., PubMed) sources. The *APOE-ε4* genotype decreases SIRT1 and insulin signalling in neurons and decreases brain microvascular endothelial cell (BMEC) in mice. Exercise training increases brain glucose metabolism in mice and humans. The impacts of *APOE-ε4* and exercise on BMEC are not well established.

Added value of this study

We found the *APOE-ε4* genotype reduces BMEC barrier function by reducing SIRT1 and decreases BMEC glucose metabolism by impairing insulin signalling. Finally, we found serum from exercise-trained individuals has genotype-dependent dimorphic effects on SIRT1 but does not alter BMEC barrier function or metabolism.

Implications of all the available evidence

This manuscript demonstrates two mechanisms through which the *APOE-ε4* genotype directly impairs BMEC metabolism and function which can be leveraged to develop therapeutics against AD and calls for further studies of the mechanisms behind exercise benefits in prevention of AD.

In vitro, APOE-ε4 astrocytes had decreased glycolysis but increased pentose phosphate pathway (PPP) activity as compared to *APOE-ε3* astrocytes, leading to increased lipid and nucleotide biosynthesis.[11] Notably, none of these studies examined mechanisms through which the *APOE* genotype itself regulates BMEC barrier function or cellular metabolism.

Exercise training in healthy older adults increases cerebral blood flow,[12] reduces hippocampal atrophy,[13] and increases brain glucose metabolism,[14] each of which reduces AD risk. Exercise training also improves Aβ clearance in rodents[15] and may reduce humans plasma Aβ levels as well.[16] From a mechanistic standpoint, exercise elevates circulating irisin, lactate, and cathepsin B, which are all hypothesised to increase brain derived neurotrophic factor (BDNF),[17–20] a molecule that supports neuronal growth, synaptic plasticity, learning, and memory.[21,22] Past studies primarily focused on how exercise training improves neuronal signalling to improve cognition. However, little is known of how exercise alters BMEC function, which is of particular importance because BMEC are directly in contact with the circulation and therefore act as first responders to the benefits of exercise training.

The goal of this study was to investigate *APOE-ε4* induced mechanisms of BMEC barrier and metabolic dysfunction, and the role of exercise training in counteracting these deficits. We used iPSC-derived BMEC-like cells to investigate the role of *APOE* genotype alone in BMEC barrier function and metabolism and then added human serum from healthy older adults (ages 65–80) collected pre- and post-6 months exercise training before re-evaluating barrier function and metabolism. Here, we outline two mechanisms through which *APOE-ε4* regulates barrier function and glucose metabolism: reduced sirtuin 1 (SIRT1) and reduced insulin signalling. We then investigate how human serum collected pre- and post- 6 months of exercise training alters these pathways in BMEC. We used CRISPR/Cas9 to generate induced pluripotent stem cells (iPSC) homozygous for the *APOE-ε3* and *-ε4* alleles. We then differentiated the iPSC into BMEC (hiBMEC), which have better barrier function and similar glucose metabolism to primary BMEC.[23] Using the *APOE-ε3* and *-ε4* hiBMEC, we studied how the *APOE-ε4* genotype leads to barrier and glycolytic deficits. Finally, using serum collected from older adults pre- and post-6 months of exercise training, we assessed how genotype-matched exercise-trained serum impacts *APOE-ε3* and *-ε4* hiBMEC barrier function and metabolism.

Methods

Ethics

This work was conducted in line with the ARRIVE reporting guidelines.[24] All experimental procedures were approved by the Institutional Review Board of University of Maryland, College Park and human serum was collected in this study in accordance with the approved clinical trial NCT03727360. All donors provided written informed consent prior to participation.

iPSC culture

IMR90 iPSC (RRID: CVCL_C437)[25] were cultured on Matrigel (Corning, 354230) and maintained in mTeSR–Plus medium (STEMCELL Technologies, 100-0276). iPSC were passaged after reaching 70% confluence using Versene (Thermo Fisher, 15040066).

CRISPR/Cas9

IMR90 iPSC are homozygous for the *APOE-ε3* allele.[26] Clustered regularly interspaced short palindromic repeats (CRISPR)/Cas9 technology was used to induce a point mutation and alter the iPSC to be homozygous for the *APOE-ε4* allele based on previously established protocols.[27] Small guide RNA (sgRNA; Table 1) targeting rs429358 (IDT) was resuspended to 100 μM in Resuspension Buffer R (Thermo Fisher, MPK10096). Single-stranded oligodeoxynucleotides (ssODN) were also resuspended to 200 μM in Resuspension Buffer R. iPSC at 80% confluence were dissociated using TrypLE (Thermo Fisher, 12605010), centrifuged at 300×*g* for 5 min, then resuspended at 13.5 × 10^6 cells/mL in 100 μL of Resuspension Buffer R. 3 μL sgRNA, 2 μL

Item	Sequence
sgRNA	GCGGACATGGAGGACGTGTGCGG
ssODN	AGGAGCTGCAGGCGGCGCAGGCCCGGCTGGGCGCGGACATG GAGGATGTACGTGGCCGCCTGGTGCAGTACCGCGGCGAGGT GCAGGCCATGCTCGGCCAG
APOE-ε3 Forward	GTAAAACGACGGCCAGTGTCTCTGTCTCCTTCTCTC
APOE-ε3 Reverse	AGGTCATCGGCATCGCGGA
APOE-ε4 Forward	GTAAAACGACGGCCAGACGAGACCATGAAGGAGTTG
APOE-ε4 Reverse	ACACTGCCAGGCGCTTCTG

Table 1: **CRISPR/Cas9 and genotyping sequences.**

ssODN, 3 µL Alt-R Cas9 Nuclease V3 (IDT), and 7 µL cell suspension were combined and electroporated using a Neon Transfection Instrument (Thermo Fisher) at 1100 V, with 2 pulses of 30 ms each. Following electroporation cells were replated on Matrigel coated plates in mTeSR–Plus medium supplemented with 10 µM Y-27632 (Tocris, 1254) and 1:1000 Alt-R HDR Enhancer (IDT, 1081072).

iPSC expansion and genotyping

Following CRISPR editing, iPSC were cultured to 70% confluence, passaged using Accutase (Thermo Fisher, A1110501), replated at 15,000 cells/well, and allowed to grow from single cells into colonies in which each cell was a replicate of a single cell. Individual colonies were expanded, and DNA was sequenced to find successfully edited colonies. DNA was isolated using a Quick-DNA Miniprep Plus Kit (Zymo Research; D4068) following manufacturer's protocol. PCR reactions were run using AmpliTaq Gold 360 Master Mix (Thermo Fisher; 4398881) and associated protocols. Samples were thermally cycled using a Pro Flex Thermal Cycler (Thermo Fisher) with an initial 10-min activation at 95 °C followed by 40 cycles of 30 s denaturing at 95 °C, 30 s of annealing at 70 °C, and 60 s/kb at 72 °C. A final extension was performed at 72 °C for 7 min before cooling back to 4 °C. Samples were then sent to Genewiz (Azenta Life Sciences) for sequencing. Sequencing results were processed through the Synthego ICE CRISPR Analysis tool and successful homozygous *APOE-ε3* (isogenic controls) and *-ε4* (edited samples) were expanded and frozen in liquid nitrogen for future use.

hiBMEC differentiation

hiBMEC were differentiated following established protocols.[28,29] iPSC at 70% confluence were passaged using Accutase onto Matrigel coated plates at 150,000 cells/well in mTeSR–Plus medium containing 10 µM Y-27632. Over the next four days media was replaced daily with E6 Medium (STEMCELL Technologies, 05946). On the fifth day, media was replaced with Neurobasal medium (Thermo Fisher, 2110304) supplemented with 10 mM glucose (Millipore Sigma, G5767), 4.5 mM glutamine (Fisher Scientific, 25-030-081), 2% B27 (Thermo Fisher, 17504001), 20 ng/mL basic fibroblast growth factor (bFGF; Peprotech, 100-18B), and 10 µM retinoic acid (RA; Millipore Sigma, R2625-50MG). Media was not changed on the sixth day. On the seventh day, cells were dissociated using Accutase and re-plated at 1×10^6 cells/cm^2 on 0.4 µm Transwell Filters (Corning, 3460), 12-well plates (CELLTREAT, 229112), or 96-well plates (Cellvis, P96-1.5P) coated with extracellular matrix (ECM) containing 0.4 mg/mL collagen IV (Millipore Sigma, C7521) and 0.1 mg/mL fibronectin (Millipore Sigma, F2006). For all experiments, cells were cultured for 2 days following subculture in Neurobasal medium with 2% B27, then treated with any applicable treatments for 24 h before collecting endpoint experimental outputs. In experiments comparing *APOE-ε3* and *-ε4* genotypes, biological replicates were collected from separate cell culture wells.

Exercise training

Adults between the ages of 60 and 80 years old were recruited in compliance with clinical trial NCT03727360. Participants included in the trial were screened for signs of mild cognitive impairment, dementia, and neurological illness, and were deemed cognitively healthy. Inclusion in the trial required participants to be physically inactive, meaning they did not partake in physical activity more than 2 days a week over the past 6 months. Participants were excluded from the trial if they had history or evidence of cardiovascular disease, cerebrovascular disease, or pulmonary disease. During the 6-month clinical trial, each participant was randomly assigned to either a low or a moderate intensity exercise training intervention. At the start of the trial, the peak rate of oxygen consumption ($\dot{V}O_{2peak}$) was measured in each participant to quantify their cardiorespiratory fitness. To minimise potential confounders, all low and moderate intensity participants began each workout with the same 20-min warmup. Following the warmup, the moderate intensity group completed a moderate intensity aerobic exercise regimen while the participants in the low intensity group completed a set of mild resistance exercises. For both the low and moderate intensity groups, exercise duration and frequency increased over the course of the study, starting with 10 min of exercise one day a week and finishing with 60 min of exercise four days per week. $\dot{V}O_{2peak}$ testing was then repeated at the end of the 6-month trial (Table 2).

Human serum collection and use

Human serum was collected during clinical trial NCT03727360 and banked for this ancillary study. At the start and finish of the trial, 6 mL of whole blood was

Genotype	Training condition	Time point	$\dot{V}O_{2peak}$	$\Delta\dot{V}O_{2peak}$
APOE ε3	Low Intensity	pre	17.23 (±1.90)	0.63 (±1.60)
		post	17.33 (±0.46)	
	Moderate Intensity	pre	15.96 (±4.38)	0.10 (±1.81)
		post	17.86 (±4.96)	
APOE ε4	Low Intensity	pre	18.35 (±6.21)	1.67 (±4.05)
		post	20.02 (±4.14)	
	Moderate Intensity	pre	12.80 (±3.88)	2.00 (±3.85)
		post	17.73 (±3.85)	

Table 2: $\dot{V}O_{2peak}$ **of individuals pre- and post-exercise training.**

drawn from each participant in Vacutainer Serum Separator Tubes (SST; BD, 367989), and deidentified for downstream analyses. To isolate serum, whole blood in SST tubes was left undisturbed at room temperature for 20 min, then centrifuged at 2000×*g* for 10 min at 4 °C. Serum was then aliquoted and stored at –80 °C until use. Sample size was determined by the number of *APOE-ε4* serum samples collected during the duration of this trial. Of the 40 serum donors included in the trial, 9 had at least one copy of the *APOE-ε4* allele, matching with estimated population allele frequencies.[30] Researchers responsible for the collection and preparation of serum samples were blinded to the *APOE* genotype of the donors, and all serum samples were deidentified before being transferred to the researchers performing cell culture experiments. Researchers performing experiments were not blinded to *APOE* genotype to ensure even numbers of each group. To ensure equal sample sizes in each group, 9 *APOE-ε3* homozygous donors were selected at random for downstream experiments. For all experiments, *APOE-ε3* and *-ε4* hiBMEC were treated with 20% genotype-matched human serum for 24 h before downstream analysis. Serum donor demographics are reported (Table 3). In

	APOE-ε3 (n = 9)	*APOE-ε4* (n = 9)
Donor sex		
Male	0 (0%)	3 (33%)
Female	9 (100%)	6 (66%)
Donor genotype		
Homozygous	9 (100%)	1 (11%)
Heterozygous	0 (0%)	ε2/ε4: 2 (22%) ε3/ε4: 6 (66%)
Donor race		
Undisclosed	0 (0%)	1 (11%)
White	6 (67%)	5 (56%)
Black/African American	2 (22%)	3 (33%)
Asian	1 (11%)	0 (0%)
Age at consent		
Average (±SD)	65.3 ± 5.0	65.1 ± 3.9

Table 3: **Serum donor demographics.**

experiments with serum treatment, biological replicates were cells treated with serum from donors of the same genotype.

ELISA

Enzyme-linked immunosorbent assays (ELISAs) were used to quantify SIRT1 (Thermo Fisher, EH427RB) and APOE (Thermo Fisher, EHAPOE). For both assays aliquots of serum were thawed on ice, and assays were run following manufacturer's protocols. Absorbances were read at 450 nm using a Tecan Spark Multimode Microplate Reader, and concentrations were calculated based on standards included in the assay kits.

TEER

To measure transendothelial electrical resistance (TEER), hiBMEC were subcultured onto 0.4 μm ECM-coated Transwell filters in Neurobasal medium with 2% B27, 20 ng/mL bFGF, and 10 μM RA. Every day post-subculture, TEER was measured in triplicate using STX2-Plus electrodes and the Epithelial Volt/Ohm Meter 3 (EVOM3; World Precision Instruments).

Immunostaining and junction analyser program

hiBMEC in 96-well plates were fixed with either 4% paraformaldehyde (PFA; Millipore Sigma, P6148) (GLUT1, ZO-1, occludin) or ice-cold 100% methanol (Millipore Sigma, 646377) (claudin-5) for 20 min. Cells were then blocked and permeabilised for 1 h at room temperature in 5% normal goat serum (Millipore Sigma, S26) in PBS supplemented with 0.2% Triton X-100 (Alfa Aesar, A16046), then incubated overnight at 4 °C in primary antibodies (Table 4). The next day, cells were incubated in either Alexa Fluor 594 goat anti-rabbit or Alexa Fluor 488 goat anti-mouse secondary antibodies (1:1000) and Hoechst (1:2000) for 1 h at room temperature. Z-stacks of the junctions were captured on an Eclipse Ti2 spinning disk confocal microscope (Nikon) at 60× magnification. 3 images were taken per well, and 9 wells were imaged per treatment group. Maximum intensity projections were created in Fiji of each image. The Junction Analyser Program (JAnaP)[31] was then used to characterise the percent of continuous junctions surrounding each cell. Continuous junctions were classified as areas along the traced edge of the cell with >15 pixels of continuous labelling. 5 cells were quantified per image.

Western Blot

hiBMEC were lysed in RIPA Buffer (Thermo Fisher, 89901) containing Halt Protease and Phosphatase Inhibitor (Fisher Scientific, PI78440) and Deacetylation Inhibition Cocktail (Santa Cruz Biotechnology, sc-362323). Protein was quantified using a bicinchoninic acid assay (Thermo Fisher, 23225), and 35 μg protein was combined with 7.5 μL sample buffer (Thermo Fisher, NP0008) and 3 μL reducing agent (Thermo Fisher, NP0009). Samples were either warmed to 37 °C

Antibody	Manufacturer	Catalogue number	Dilution	RRID
GLUT1	Thermo Fisher Scientific	21829-1-AP	1:100 (Immunostaining) 1:4000 (Western Blot)	AB_10837075
HK1	Santa Cruz Biotechnology	sc-46695	1:1000 (Western Blot)	AB_627721
HK2	Santa Cruz Biotechnology	sc-374,091	1:1000 (Western Blot)	AB_10917915
PFKFB3	Cell Signaling Technology	13123S	1:1000 (Western Blot)	AB_2617178
GAPDH	Thermo Fisher Scientific	437,000	1:1000 (Western Blot)	AB_10374327
LDH	Santa Cruz Biotechnology	sc-133,123	1:1000 (Western Blot)	AB_2134964
β-Actin	Santa Cruz Biotechnology	sc-47778	1:1000 (Western Blot)	AB_626632
INSR	Santa Cruz Biotechnology	sc-57342	1:1000 (Western Blot)	AB_784102
SIRT1	Cell Signaling Technology	9475S	1:1000 (Western Blot)	AB_2617130
APOE	Thermo Fisher Scientific	MA516146	1:1000 (Western Blot)	AB_11157884
GFAT	Cell Signaling Technology	5322S	1:1000 (Western Blot)	AB_10699031
G6PD	Cell Signaling Technology	12263S	1:1000 (Western Blot)	AB_2797861
Na/K ATPase	Santa Cruz Biotechnology	sc-28800	1:1000 (Western Blot)	AB_290063
Akt	Cell Signaling Technology	9272S	1:1000 (Western Blot)	AB_329827
p-Akt	Cell Signaling Technology	9271S	1:1000 (Western Blot)	AB_329825
ZO-1	Cell Signaling Technology	13663S	1:100 (Immunostaining)	AB_2798287
Occludin	Cell Signaling Technology	91131S	1:100 (Immunostaining)	AB_2934013
Claudin 5	Thermo Fisher Scientific	35–2500	1:100 (Immunostaining)	AB_2533200
Anti-mouse IgG (H + L), HRP Conjugate	Promega	W4021	1:2000 (Western Blot)	AB_430834
Anti-rabbit IgG (H + L), HRP Conjugate	Promega	W4011	1:2000 (Western Blot)	AB_430833
Goat anti-rabbit IgG (H + L) 594	Thermo Fisher Scientific	A-11012	1:1000 (Immunostaining)	AB_2534079
Goat anti-mouse IgG (H + L) 488	Thermo Fisher Scientific	A-11001	1:1000 (Immunostaining)	AB_2534069
Hoechst	Thermo Fisher Scientific	PI62249	1:2000 (Immunostaining)	AB_2651133

Table 4: **Antibodies.**

(for glucose transporter 1 (GLUT1) only) or boiled at 70 °C (for all other proteins) for 5 min and loaded into 4–12% Bis Tris gels (Thermo Fisher, NP0323). Protein was transferred to either polyvinylidene fluoride (for GLUT1; Thermo Fisher, IB23001) or nitrocellulose (for all other proteins, Thermo Fisher, IB24001) membranes using an iBlot2 (Thermo Fisher, IBL21001). Polyvinylidene fluoride membranes were blocked in 5% milk in tris buffered saline (TBS; Fisher Scientific, BP24711) with 0.5% Tween 20 (Thermo Fisher, 85113) for 1 h, incubated in primary antibodies (Table 4) overnight at 4 °C in 1% bovine serum albumin (BSA) in TBS with 0.5% Tween 20, and then incubated for 2 h at room temperature in secondary antibody in 1% BSA in TBS with 0.5% Tween 20. Membranes for all other proteins were blocked for 1 h at room temperature in 5% bovine serum albumin (BSA; Millipore Sigma, 126609) in PBS with 0.5% Tween 20, then incubated in primary antibodies (Table 4) overnight at 4 °C in 1% BSA in PBS with 0.5% Tween 20, and secondary antibodies for 2 h at room temperature in 1% BSA in PBS with 0.5% Tween 20. Membranes were imaged using an Alpha Inotech Fluorchem Imager (Protein Simple) and analysed using AlphaView.

SIRT1 activity assay

SIRT1 activity was quantified using a fluorometric SIRT1 activity assay (abcam, ab156065) run according to manufacturer's protocols. 2 technical replicates were run for each sample. Protein concentrations from *APOE-ε3* and *-ε4* hiBMEC were quantified using a BCA assay (Thermo Fisher, 23225). SIRT1 fluorescence readings were normalised to total protein levels for each biological replicate.

Extracellular metabolite flux measurements

Glucose and glutamine uptake and lactate and glutamate secretion, as well as transport of each metabolite, were measured using a Yellow Springs Instruments (YSI) 2950 (Yellow Springs Instruments, 527690). Media samples were collected from either 12 well plates or both the apical and basolateral chambers of Transwell inserts at 0- and 24-h. Glucose, lactate, glutamine, and glutamate measurements were measured on the YSI. Metabolite uptake was calculated by subtracting metabolite concentrations at 24 h from the initial concentrations. Metabolite secretion was calculated by subtracting initial concentrations from the 24-h metabolite concentrations.

Seahorse glycolytic rate assay

A Seahorse glycolytic rate assay (GRA; Agilent, 103344-100) was used to evaluate rates of glycolysis. hiBMEC were seeded at 50,000 cells/well in 96-well Seahorse assay plates. On the day of the assay, cells were washed once with fresh Seahorse DMEM, and then incubated

for 1 h in Seahorse DMEM supplemented with 10 mM glucose, 2 mM glutamine, 1 mM pyruvate, and 2% B27 before running the GRA in a Seahorse XFe96 following manufacturer's instructions.

Membrane fractionation

To quantify GLUT1 levels in the cell membrane of *APOE-ε3* and *-ε4* hiBMEC, a Mem-PER Plus Membrane Protein Extraction Kit (Thermo Fisher, 89842) was used. *APOE-ε3* and *-ε4* hiBMEC cultured in 12-well plates were lysed in membrane permeabilisation buffer supplemented with Halt Protease and Phosphatase Inhibitor. Samples were agitated for 10 min at 4 °C and then centrifuged at 17,000×*g* for 10 min at 4 °C. Supernatant containing the cytosolic proteins was removed and stored on ice. The pellet was then resuspended in membrane solubilisation buffer, agitated for 30 min at 4 °C, and then centrifuged at 17,000×*g* for 30 min at 4 °C. Protein was quantified, and western blot was run following previously described protocols.

Mass spectrometry

APOE-ε3 and *-ε4* hiBMEC were cultured in Neurobasal medium supplemented with 8.5 mM glucose, 4.5 mM glutamine, and 2% B27 for 2 days following subculture. Cells were then incubated for 24 h in Neurobasal medium (±20% human serum) supplemented with 4.5 mM glutamine and 8.5 mM U-$^{13}C_6$-glucose (Fisher Scientific, NC9207695). To extract metabolites, cells were incubated in 80:20 methanol:water for 15 min at –80 °C and then centrifuged at 16,000 g for 10 min to pellet debris. Mass spectrometry was performed by the University of Colorado School of Medicine Metabolomics Core. Samples were randomised and a Vanquish ultra-high performance liquid chromatograph (UHPLC; Thermo Fisher) was used to inject 8 µL of each sample into a Q Exactive Mass Spectrometer (MS).[32] Eluent was introduced to the MS via electrospray ionisation. The MS scanned 2 µscans over 65–950 *m/z*. Maven (Princeton University) and the KEGG database were used to manually annotate the metabolites, and peak quality was determined using technical mixes, blanks, and ^{13}C natural abundances.[33] The IsoCor Python package was used to correct isotope labelling,[34] and metabolite pool sizes were analysed using Metaboanalyst 6.0.[35] Metaboanalyst was used to generate partial least squares discriminant analysis (PLS-DA) plots wherein principal component 1 (PC1) on the x-axis is derived from the variables contributing to the greatest amount of variance in the dataset, while PC2 on the y-axis is derived from the variables contributing to greatest amount of variance once those in PC1 are removed from the dataset. The percent variance accounted for by each PC is noted on the axis.

Metabolic flux analysis

Isotopomer Network Compartmental Analysis (INCA) 2.2 was used to perform metabolic flux analysis (MFA).[36,37] INCA is a user-friendly MATLAB based tool which uses experimental isotope datasets, extracellular fluxes, and a model of metabolic network reactions to estimate intracellular fluxes. INCA searches to identify the flux parameters for the intracellular fluxes to minimise the sum-of-squared residuals (SSR) between the experimental and computationally stimulated fluxes. The network model used here is based on similar models we developed for endothelial cells[38] and includes reactions at isotopic and metabolic steady state for glycolysis, the PPP, the tricarboxylic acid (TCA) cycle, and amino acid metabolism. Briefly, to estimate the intracellular fluxes the ^{13}C isotope distribution data for *APOE-ε3* and *-ε4* hiBMEC measured using mass spectrometry were corrected for the natural abundance of labelled and unlabelled atoms and input into the INCA software. The model was bounded by extracellular fluxes for glucose, glutamine, lactate, and glutamate measured using the YSI bioanalyser (converted to nmol/hr). The extracellular fluxes and isotope labelling data were fitted to the metabolic network map by generating a random initial flux guess and iterated until the best fit between the experimental and simulated fluxes was achieved. The fluxes were predicted using the Levenberg–Marquardt gradient descent algorithm[37] and were repeated 100 times starting from random initial points to improve the statistical chance of finding a global optimum. Fit was based on n-p degrees of freedom, where n is the number of independent measurements and p is the number of fitted parameters. The final model contained 67 reactions. The number of fitted parameters differed between models, so the *APOE-ε3* hiBMEC model had 79 degrees of freedom and the *APOE-ε4* model had 76 degrees of freedom. The parameter continuation function was used by INCA to generate the confidence intervals.

Measurement error was set to a minimum of 1% based on previous recommendations.[39] The distribution of residual error is expected to follow a normal distribution, and deviations from this suggest either inaccuracies in the model or gross measurement error. All isotopomers were scrutinised to identify poorly fitting measurements. Those that could not be explained by biochemically feasible reactions were rescaled to have an error of up to 5% to improve model fit and ensure a normal distribution of residual error. To minimise the SSR, the accepted error for some of the metabolites (GABA, ribose-5-phosphate, glutamate, citrate, and malate) was increased from 1% to 5%. For all other metabolites the accepted error was kept at 1%. To improve the accuracy of the flux predictions, experimental data from two different glucose labelling experiments were input into the model in parallel.

The final MFA output produced a set of possible flux predictions for each model. However, there is a degree of uncertainty in these predictions which allows each flux to take on a range of values. The parameter

continuation function was used by INCA to generate 95% confidence intervals which estimate upper and lower boundaries for each metabolic reaction. Metabolic reactions without overlapping 95% confidence intervals were considered significantly different between the two genotypes, as is standard practice in MFA.[38]

Statistics

Statistics were analysed in GraphPad Prism. Data were not assumed to be normally distributed, so non-parametric statistical tests were used. Non-parametric Mann–Whitney tests were used to compare *APOE-ε3* and *-ε4* hiBMEC. Non-parametric Kruskal–Wallis tests were used to compare effects of insulin and wortmannin. Comparisons between *APOE* genotype and pre-and post-exercise training serum were analysed using repeated measures two-way ANOVA with Fisher's Least Significant Difference test. p-values <0.05 were considered statistically significant.

Role of funders

Funders were not involved in study design, data collection, data analysis, data interpretation, or writing of the report.

Results

The *APOE-ε4* genotype is associated with BBB breakdown and brain glucose hypometabolism. We therefore explored how the *APOE-ε4* genotype impacts barrier strength and glucose metabolism in hiBMEC and how these metabolic changes propagate into systemic metabolic differences between *APOE-ε3* and *-ε4* hiBMEC. Then, we investigated how exercise training, as a preventative therapeutic against AD, changes hiBMEC barrier function and metabolism.

hiBMEC with the *APOE-ε4* genotype had reduced barrier function

APOE-ε4 carriers have elevated BBB permeability relative to *APOE-ε3* homozygotes.[5] We began by determining if this phenotype also occurred in hiBMEC. CRISPR/Cas9 was used to insert a point mutation and thereby change iPSC homozygous for the *APOE-ε3* allele to iPSC homozygous for the *APOE-ε4* allele (Fig. 1a). These iPSC were then differentiated to hiBMEC,[28,29] and barrier function was assessed using TEER and immunofluorescence. TEER was 36% lower in *APOE-ε4* hiBMEC compared to *-ε3* hiBMEC ($p < 0.0001$ [Mann–Whitney Test]; Fig. 1b). Tight junction protein ZO-1 continuity was 8.7% lower in *APOE-ε4* hiBMEC compared to *-ε3* hiBMEC ($p < 0.0001$ [Mann–Whitney Test]), suggesting that loss of ZO-1 may contribute to BBB breakdown in *APOE-ε4* BMEC. Continuity of tight junction proteins occludin and claudin-5 did not significantly differ by genotype (Fig. 1c and d).

Reduced SIRT1 contributed to lower barrier function in *APOE-ε4* compared to *-ε3* hiBMEC

We next investigated mechanisms through which the *APOE-ε4* genotype caused lower barrier function than the *APOE-ε3* genotype. In neuroblastoma and glioblastoma cells, the *APOE-ε4* protein directly suppresses transcription of SIRT1.[40,41] Increasing SIRT1 decreases endothelial permeability through increased ZO-1[42] and claudin-5.[43] Therefore, we hypothesised that *APOE-ε4* hiBMEC have lower SIRT1 than *APOE-ε3* hiBMEC, which impairs barrier function by decreasing ZO-1 junction continuity.

Western blots for SIRT1 demonstrated that *APOE-ε4* hiBMEC had 27% less SIRT1 protein compared to *APOE-ε3* hiBMEC ($p = 0.0188$ [Mann–Whitney Test]; Fig. 2a and b). A fluorometric SIRT1 activity assay showed SIRT1 activity was also 10% lower in *APOE-ε4* compared to *-ε3* hiBMEC ($p = 0.0030$ [Mann–Whitney Test]; Fig. 2c). To examine if the lower SIRT1 in the *APOE-ε4* hiBMEC contributed to reduced barrier function, we modulated SIRT1 activity using a SIRT1 specific inhibitor, Ex-527. 10 μM Ex-527 decreased SIRT1 activity by 12% ($p = 0.0570$ [Mann–Whitney Test]; Fig. 2d). Then, we used immunofluorescent labelling and the Junction Analyser Program[31] to examine how SIRT1 inhibition altered hiBMEC barrier function. Ex-527 decreased ZO-1 continuity by 26% ($p < 0.0001$ [Mann–Whitney Test]; Fig. 2e and f) but did not significantly alter claudin-5 continuity (Fig. 2g and h).

APOE-ε4 hiBMEC had reduced glucose metabolism relative to *APOE-ε3* hiBMEC

In addition to modulating barrier function, SIRT1 is known to regulate glycolysis. Glucose hypometabolism is a hallmark of AD, and low SIRT1 may decrease glycolysis through reduced GLUT1[44] and HK2.[45] We used YSI and Seahorse Glycolytic Rate assays to assess if glycolytic rates were different between *APOE-ε3* and *-ε4* hiBMEC. *APOE-ε4* hiBMEC had 31% lower glucose uptake than *APOE-ε3* hiBMEC ($p < 0.0001$ [Mann–Whitney Test]; Fig. 3a), as measured by YSI. Lactate secretion was 9% lower in *APOE-ε4* hiBMEC, although this was not statistically significant ($p = 0.0780$ [Mann–Whitney Test]; Fig. 3b). The basal glycolytic rate, measured by the Seahorse glycolytic proton efflux rate (GlycoPER), was 20% lower in *APOE-ε4* hiBMEC than *-ε3* hiBMEC ($p < 0.0001$ [Mann–Whitney Test]; Fig. 3c. Overall, these data indicate that *APOE-ε4* hiBMEC have a decreased glycolytic rate compared to *APOE-ε3* hiBMEC.

Next, we analysed glycolytic enzymes by Western blot to evaluate which glycolytic enzymes contributed to lowered glycolysis in *APOE-ε4* hiBMEC (Fig. 3d) Glucose entry into BMEC primarily occurs through the glucose transporter GLUT1. GLUT1 levels were 38% lower in *APOE-ε4* hiBMEC compared to *-ε3* hiBMEC ($p = 0.0003$ [Mann–Whitney Test]; Fig. 3e). Glucose is

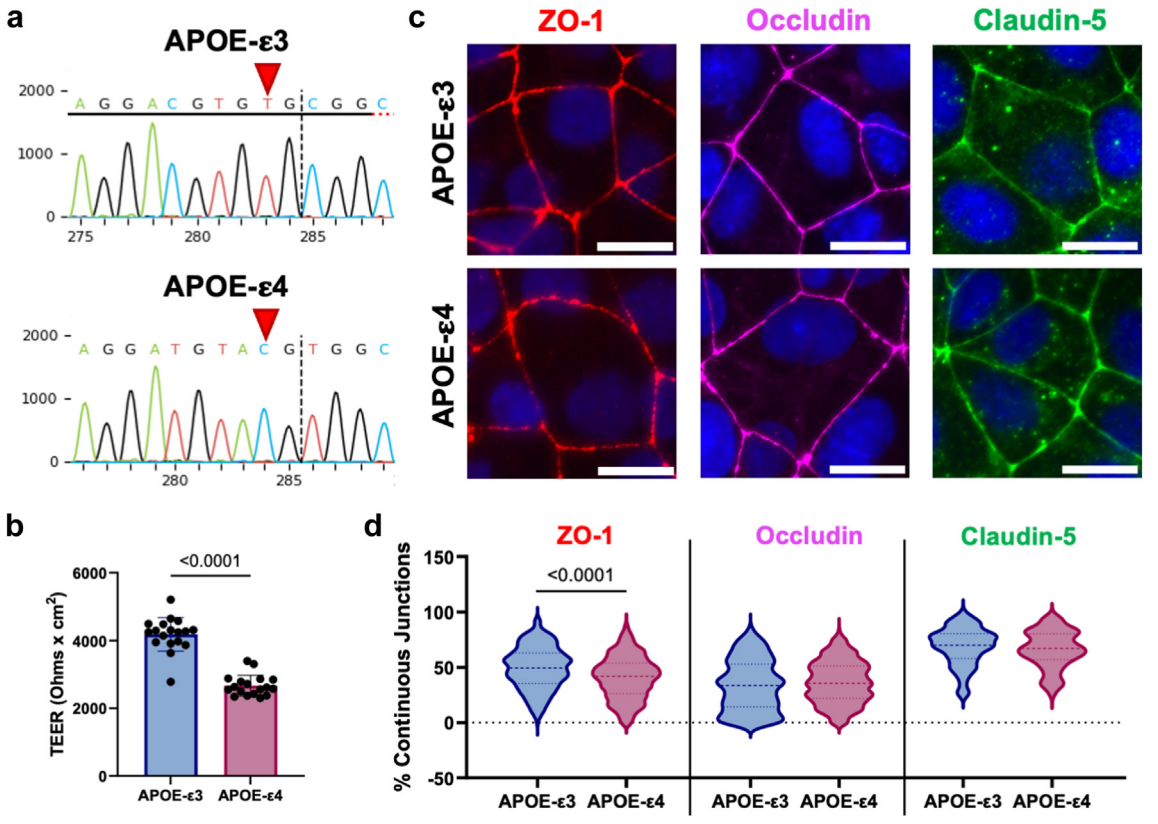

***Fig. 1: APOE-ε4* BMEC had reduced barrier function. (a)** Sequencing electropherograms of iPSC edited with CRISPR/Cas9 targeting the *APOE* gene. Red arrows indicate the nucleotide that determines the *APOE* genotype in *APOE-ε3* isogenic control iPSC and edited *APOE-ε4* iPSC. **(b)** TEER measured on *APOE-ε3* and *-ε4* hiBMEC (n = 18 samples per genotype). **(c)** Immunofluorescent labelling of tight junction proteins in *APOE-ε3* versus *APOE-ε4* hiBMEC. ZO-1 (red), occludin (magenta), and claudin-5 (green). **(d)** Percent continuous junctions quantified via Junction Analyser Program. Scale bar = 20 μm (n = 176–327 cells from 16 biological replicates). Dotted lines indicate interquartile range. Data analysed using Mann–Whitney tests.

then converted to glucose-6-phosphate by hexokinase (HK) 1 or 2. HK1 levels were similar between *APOE-ε3* and *-ε4* hiBMEC (Fig. 3F); however, HK2 was 20% lower in *APOE-ε4* compared to *-ε3* hiBMEC (p = 0.0188 [Mann–Whitney Test]; Fig. 3g). Downstream glycolytic rate limiting enzyme PFKFB3 was also 24% lower in *APOE-ε4* compared to *-ε3* hiBMEC (p = 0.0106 [Mann–Whitney Test]; Fig. 3h), while glycolytic enzymes GAPDH and LDH were unchanged between *APOE-ε3* and *-ε4* hiBMEC (Fig. 3i and j). Additionally, we measured levels of glucose-6-phosphate dehydrogenase (G6PD), the rate limiting enzyme for glucose entry into the PPP, and glutamine fructose-6-phosphate amidotransferase (GFAT), the rate limiting enzyme for glucose entry into the hexosamine biosynthesis pathway (HBP). Neither G6PD nor GFAT levels were different between *APOE-ε3* and *-ε4* hiBMEC (Fig. 3k and l).

Since lower levels of GLUT1 and HK2 in *APOE-ε4* hiBMEC correlated with lower SIRT1, we next examined if using Ex-527 to inhibit SIRT1 would inhibit glycolysis. Interestingly, the Seahorse Glycolytic Rate Assay did not demonstrate reduced hiBMEC glycolysis in response to Ex-527 (Fig. 3m), indicating that SIRT1 either does not contribute to reduced glycolysis in the *APOE-ε4* hiBMEC, or that SIRT1 only reduces glycolysis in conjunction with other metabolic regulators.

APOE-ε3 and *-ε4* hiBMEC had similar metabolite transport and polarisation

While glucose metabolism is important for energy production in BMEC themselves, BMEC are also responsible for transporting glucose from the blood into the brain for parenchymal brain cells to use as an energy source. To measure hiBMEC metabolite transport and polarisation, *APOE-ε3* and *-ε4* hiBMEC were seeded on Transwell inserts, and metabolite concentrations were measured on the apical and basolateral sides of the insert (Supplementary Fig. S1A). After 24 h, basolateral glucose concentrations were ~8.5 mM glucose for both *APOE-ε3* and *-ε4* hiBMEC; however, the apical glucose

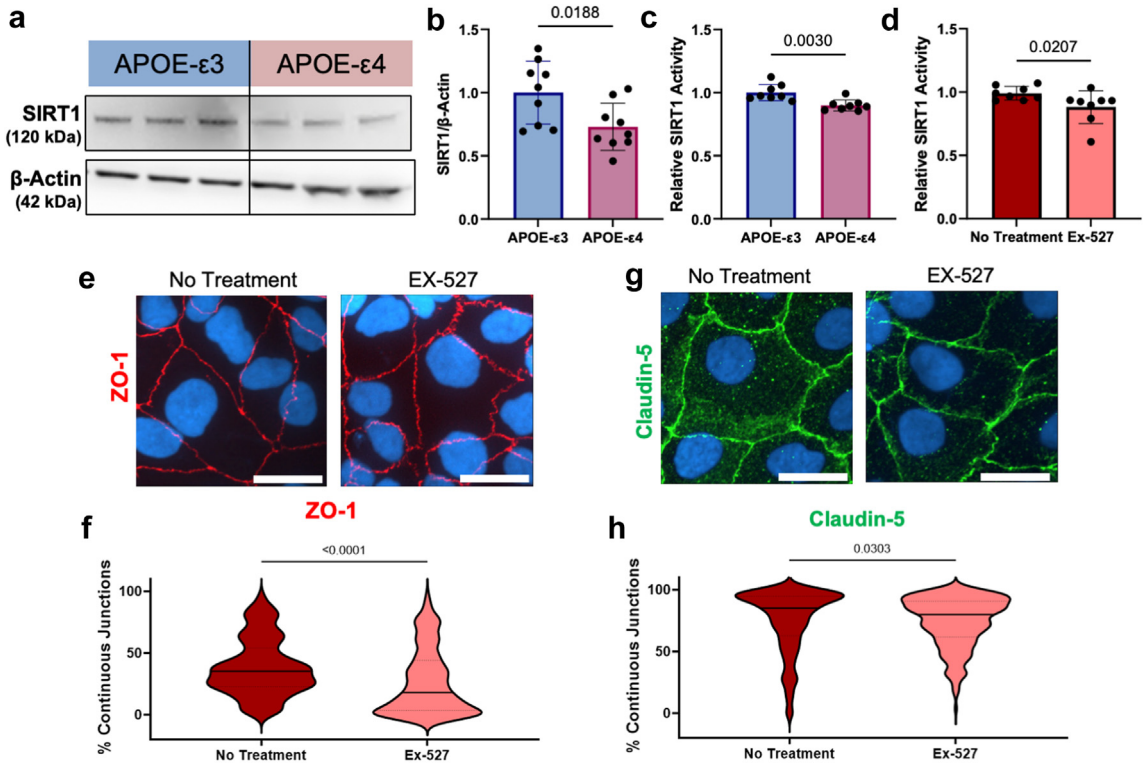

Fig. 2: **SIRT1 was lower in *APOE-ε4* hiBMEC, and SIRT1 inhibition decreased barrier function in hiBMEC. (a)** Representative Western blot and **(b)** quantification of SIRT1 relative to β-Actin in *APOE-ε3 and -ε4* hiBMEC. Data were normalised to *APOE-ε3* (n = 9 samples per genotype) **(c)** Relative SIRT1 activity measured using a SIRT1 activity assay and normalised to *APOE-ε3* hiBMEC (n = 8 samples per genotype). **(d)** SIRT1 activity in hiBMEC treated with 10 μM EX-527 for 24 h relative to untreated hiBMEC (n = 8 samples per condition). Representative confocal microscopy images of tight junction proteins **(e)** ZO-1 (red) and **(g)** claudin-5 with **(f, h)** quantification of junction continuity by the Junction Analyser program (n = 225–251 cells per condition). Data analysed using a Mann–Whitney Test.

concentration was 6.3% higher in *APOE-ε4* hiBMEC compared to *APOE-ε3 hiBMEC* ($p < 0.0001$ [Two-Way ANOVA]), indicating reduced glucose uptake in *APOE-ε4* hiBMEC (Supplementary Fig. S1B). Glucose was polarised in both *-ε3* and *APOE-ε4* hiBMEC, with higher glucose concentration in the basolateral compartment. Lactate was also polarised in both cell types, with higher lactate concentration in the apical compartment. *APOE-ε4* hiBMEC secreted 25% less lactate in the apical compartment than *APOE-ε3* hiBMEC, indicating decreased glycolysis ($p < 0.0001$ [Two-Way ANOVA]; Supplementary Fig. S1C).

APOE-ε4 genotype systemically changed hiBMEC metabolism

We next investigated if the *APOE-ε4* genotype induced other metabolic changes in hiBMEC compared to *APOE-ε3* hiBMEC using metabolomics. *APOE-ε3* and *-ε4* hiBMEC were labelled with $^{13}C_6$-glucose for 24 h, and then metabolic mass spectrometry was used to identify changes in metabolite abundance and labelling patterns between the genotypes. Partial least squares-discriminant analysis (PLS-DA) indicated that *APOE-ε3* and *-ε4* hiBMEC separated primarily along component 1 (33.8%; Supplementary Fig. S2A). A variable importance plot (VIP) was then used to identify which metabolites most contributed to the PLS-DA separation (Supplementary Fig. S2B). The metabolite with the highest VIP score was UDP-N-Acetyl-D-Glucosamine (UDP-GlcNAc), the primary product of the HBP. Nucleotides including adenosine triphosphate (ATP), uridine diphosphate (UDP), cytidine triphosphate (CTP), adenosine diphosphate (ADP), and uridine triphosphate (UTP) were also elevated in *APOE-ε4* hiBMEC. Amino acids glutamine, serine, aspartate, alanine, and glutamate were all elevated in *APOE-ε3* hiBMEC, as were TCA cycle metabolites α-ketoglutarate, succinate, and fumarate.

^{13}C metabolic flux analysis predicted lower glycolytic and higher malate shuttle and reductive carboxylation fluxes in *APOE-ε4* hiBMEC

We then examined intracellular glucose metabolism by labelling *APOE-ε3 and -ε4* hiBMEC with U-$^{13}C_6$-glucose

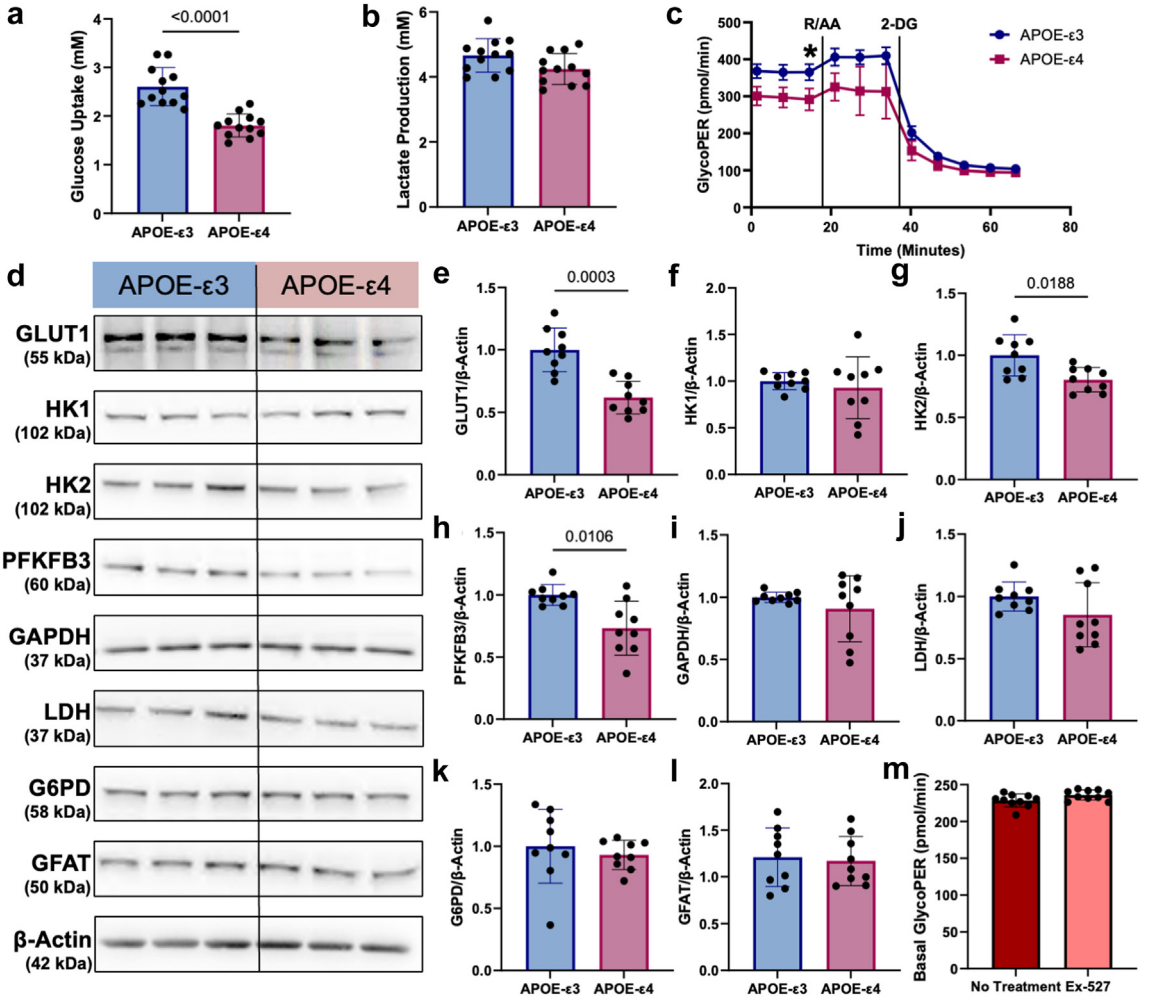

***Fig.* 3: Glycolysis and glycolytic enzymes were lower in *APOE-ε4* hiBMEC, but this decrease was not caused by reduced SIRT1.** YSI measurements of **(a)** glucose uptake and **(b)** lactate secretion over 24 h (n = 12 samples per genotype). **(c)** GlycoPER measured via Seahorse Glycolytic Rate Assay in *APOE-ε3* versus *-ε4* hiBMEC (n = 10 samples per genotype). **(d)** Representative Western blots with quantifications of **(e)** GLUT1 **(f)** hexokinase I (HK1), **(g)** hexokinase 2 (HK2), **(h)** 6-phosphofructo-2-kinase/fructose-2,6-biphosphatase 3 (PFKFB3), **(i)** glyceraldehyde 3-phosphate dehydrogenase (GAPDH), **(j)** lactate dehydrogenase (LDH), **(k)** glucose-6-phosphate dehydrogenase (G6PD), and **(l)** glutamine fructose-6-phosphate amidotransferase (GFAT) relative to housekeeper protein β-Actin (n = 9 samples per genotype). Data were normalised to *APOE-ε3* protein levels in each experiment. **(m)** Basal GlycoPER measured via Seahorse Glycolytic Rate Assay in hiBMEC treated with 10 μM EX-527 for 24 h (n = 10 samples per condition). Data were analysed using Mann–Whitney tests. *p < 0.05.

and analysed the resulting mass isotopomers. Uniformly labelled glucose is metabolised into M+2 acetyl-CoA for entry into the TCA cycle. Notable, M+2 fractional enrichment decreased in *APOE-ε4* hiBMEC for the TCA metabolites α-ketoglutarate (12% decrease, p = 0.0070 [Mann–Whitney Test]), fumarate (11% decrease, p = 0.0379 [Mann–Whitney Test]), and malate (9% decrease, p = 0.0262 [Mann–Whitney Test]) compared to *APOE-ε3* hiBMEC (Fig. 4a–c).

Decreased fractional enrichment can occur due to decreased metabolism of labelled precursors, an influx of unlabelled carbons, or a combination of both scenarios. This greatly complicates labelling data interpretation, particularly in the TCA cycle, which has multiple carbon sources and several reversible metabolic steps. To better understand differences in metabolic activity between *APOE-ε3 and -ε4* hiBMEC, we performed isotope-assisted MFA by integrating isotopomer data with extracellular flux measurements.[46] Reactions used to generate the MFA maps, and net fluxes for the *APOE-ε3* and *-ε4* MFA are included in the supplemental information (Supplementary Tables S1–S3).

We produced a simplified flux map detailing estimated fluxes through some of the metabolic pathways that were predicted to differ between *APOE-ε3* and *-ε4* hiBMEC (Fig. 4d). Data are represented through the

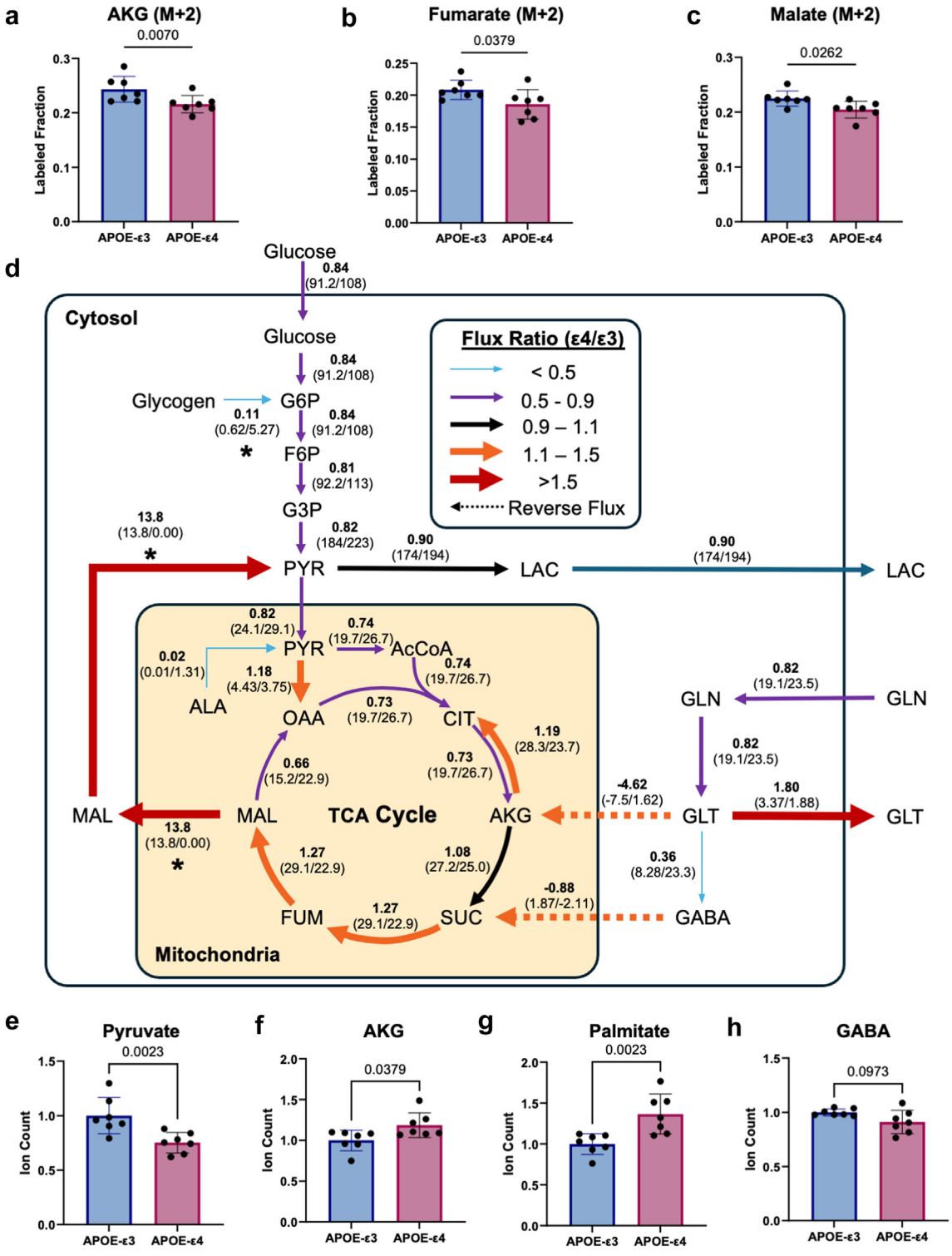

Fig. 4: **Isotope labelling and ^{13}C metabolic flux analysis showed decreased glycolysis with redirection in the TCA cycle in *APOE-ε4* hiBMEC**. Fractional enrichment for M+2 isotopomers of **(a)** α-ketoglutarate (AKG), **(b)** fumarate, and **(c)** malate. Data pooled from two independent labelling experiments, n = 7. **(d)** Metabolic flux map showing ε4/ε3 flux ratios. Reversed fluxes are shown as dashed arrows. Fluxes without overlapping 95% confidence intervals shown with an asterisk under predicted flux ratio. Total ion counts for **(e)** pyruvate **(f)** AKG **(g)** palmitate and **(h)** GABA. All samples were normalised to mean of *APOE-ε3* for the respective experiment. Data were pooled from two independent experiments (n = 7) and analysed with a Mann–Whitney test.

APOE-ε4/ε3 flux ratio, in which a flux ratio less than one indicates higher estimated flux in *APOE-ε3* hiBMEC, and a flux ratio greater than one indicates higher estimated flux in *APOE-ε4* hiBMEC. All glycolytic fluxes were reduced in *APOE-ε4* hiBMEC (flux ratio 0.81–0.84) compared to *APOE-ε3* hiBMEC up to the pyruvate branchpoint. At this metabolic junction, ^{13}C-MFA estimated a major influx of malate-sourced pyruvate in *APOE-ε4* hiBMEC, which was absent in *APOE-ε3* hiBMEC. Despite these differences, it was estimated that both genotypes directed a similar percentage of pyruvate towards oxidative respiration in the mitochondria.

Within the mitochondria, the estimated pyruvate carboxylation to oxaloacetate was higher in *APOE-ε4* hiBMEC (flux ratio = 1.18) while the estimated conversion of pyruvate dehydrogenase to acetyl-CoA was lower (flux ratio = 0.74) compared to *APOE-ε3* hiBMEC. Citrate decarboxylation to α-ketoglutarate was also estimated to be lower in *APOE-ε4* hiBMEC (flux ratio = 0.74). However, subsequent steps in the TCA cycle, including succinate, fumarate, and malate production, were estimated to be higher in the *APOE-ε4* compared to *APOE-ε3* hiBMEC (flux ratio 1.08–1.27).

Reductive carboxylation of α-ketoglutarate (α-ketoglutarate conversion to citrate) was estimated to be higher in *APOE-ε4* hiBMEC (flux ratio = 1.19). The elevated reductive carboxylation in *APOE-ε4* hiBMEC appeared to be fueled by glutamate conversion to α-ketoglutarate in the TCA cycle. In contrast, in *APOE-ε3* hiBMEC α-ketoglutarate was estimated to be converted to glutamate (flux ratio = –4.62). *APOE-ε4* hiBMEC also had an estimated lower glutamine influx and glutamine to glutamate flux (flux ratio = 0.82), and thus lower flux of glutamate to 4-aminobutanoate/GABA (flux ratio = 0.36). Interestingly, in *APOE-ε4* hiBMEC, GABA was estimated to feed into succinate, whereas in *APOE-ε3* hiBMEC the reaction was reversed (flux ratio = –0.88). Another major difference predicted by the ^{13}C-MFA was in the malate shuttle (malate conversion to pyruvate), which was not predicted to be active in *APOE-ε3* hiBMEC but was estimated to be highly active in *APOE-ε4* hiBMEC (flux ratio = 13.8).

To corroborate the ^{13}C-MFA, we examined the ion counts of key metabolites. Intracellular pyruvate ion count was 25% lower in *APOE-ε4* hiBMEC (p = 0.0023 [Mann–Whitney Test]; Fig. 4e), while α-ketoglutarate was 19% higher in *APOE-ε4* hiBMEC compared to *APOE-ε3* hiBMEC (p = 0.0379 [Mann–Whitney Test]; Fig. 4f). Reductive carboxylation of α-ketoglutarate can also feed lipogenic pathways. We found palmitate to be 37% higher in *APOE-ε4* hiBMEC (p = 0.0023; Fig. 4g). Finally, the ^{13}C-MFA predicted lower GABA synthesis and higher GABA consumption in *APOE-ε4* compared to *APOE-ε3* hiBMEC. In accordance with the model, GABA ion counts were 9% lower in *APOE-ε4* hiBMEC compared to *APOE-ε3* hiBMEC (p = 0.0973 [Mann–Whitney Test]; Fig. 4h).

Impaired insulin signalling contributed to decreased glycolysis in *APOE-ε4* hiBMEC

As decreased SIRT1 did not reduce hiBMEC glycolysis, we next investigated an alternative mechanism. The *APOE-ε4* protein inhibits insulin receptor (INSR) recycling and glycolysis in neurons.[47] We therefore hypothesised that *APOE-ε4* hiBMEC would also have reduced INSR recycling, leading to decreased GLUT1 translocation to the cell membrane, and thereby decreasing glycolytic rate. We first investigated how INSR levels differed between *APOE-ε3 and -ε4* hiBMEC by Western blot. *APOE-ε4* hiBMEC had 36% lower INSR protein levels than *APOE-ε3* hiBMEC (p = 0.0002 [Mann–Whitney Test]; Fig. 5a and b). Next, we determined how insulin signalling differed in *APOE-ε3 and -ε4* hiBMEC by treating cells with insulin and probing for phosphorylated-Akt (p-Akt) by Western blot (Fig. 5c). *APOE-ε4* hiBMEC had a 37% lower p-Akt:Akt ratio without insulin stimulation (p = 0.0186 [Two-Way ANOVA]), and an 82% lower p-Akt:Akt ratio with insulin stimulation (p = 0.0029 [Two-Way ANOVA]). While *APOE-ε3* hiBMEC increased the p-Akt:Akt ratio by 30% following insulin stimulation (p = 0.0340 [Two-Way ANOVA]), *APOE-ε4* hiBMEC did not significantly increase p-Akt:Akt ratio with insulin stimulation (Fig. 5d). These data suggest that insulin signalling is reduced in *APOE-ε4* hiBMEC, possibly through reduced INSR levels.

Next, we investigated how inhibition of insulin signalling impacted GLUT1 translocation to the membrane and glycolysis. Using membrane fractionation combined with Western blot, we showed that GLUT1 was 31% lower in *APOE-ε4* hiBMEC relative to *APOE-ε3* hiBMEC (p = 0.0017 [Two-Way ANOVA]; Fig. 5e and f). Then, we treated *APOE-ε4* hiBMEC with 10 μg/mL insulin to stimulate insulin signalling and promote GLUT1 translocation to the membrane, or 1 μM Wortmannin to inhibit PI3K in the insulin signalling pathway and thus GLUT1 membrane translocation (Fig. 5g). Insulin treatment did not increase GLUT1 membrane translocation. Wortmannin, however, decreased membrane GLUT1 by 32% (p = 0.0213 [Kruskal–Wallis Test]; Fig. 5h), indicating that decreased insulin signalling can decrease membrane GLUT1. Finally, to determine how reduced insulin signalling and membrane GLUT1 corresponded with reduced hiBMEC glycolysis, we ran a Seahorse Glycolytic Rate Assay in which hiBMEC were pretreated with insulin or Wortmannin for 30 min (Fig. 5i). Basal GlycoPER was not significantly elevated by with insulin but decreased 8.4% with Wortmannin (p = 0.0089 [Kruskal–Wallis Test]; Fig. 5j).

Serum collected post-exercise training differentially regulated SIRT1, but not barrier function, in *APOE-ε3* and *-ε4* hiBMEC

Exercise training reduces hippocampal atrophy and increases cerebral glucose metabolism associated with

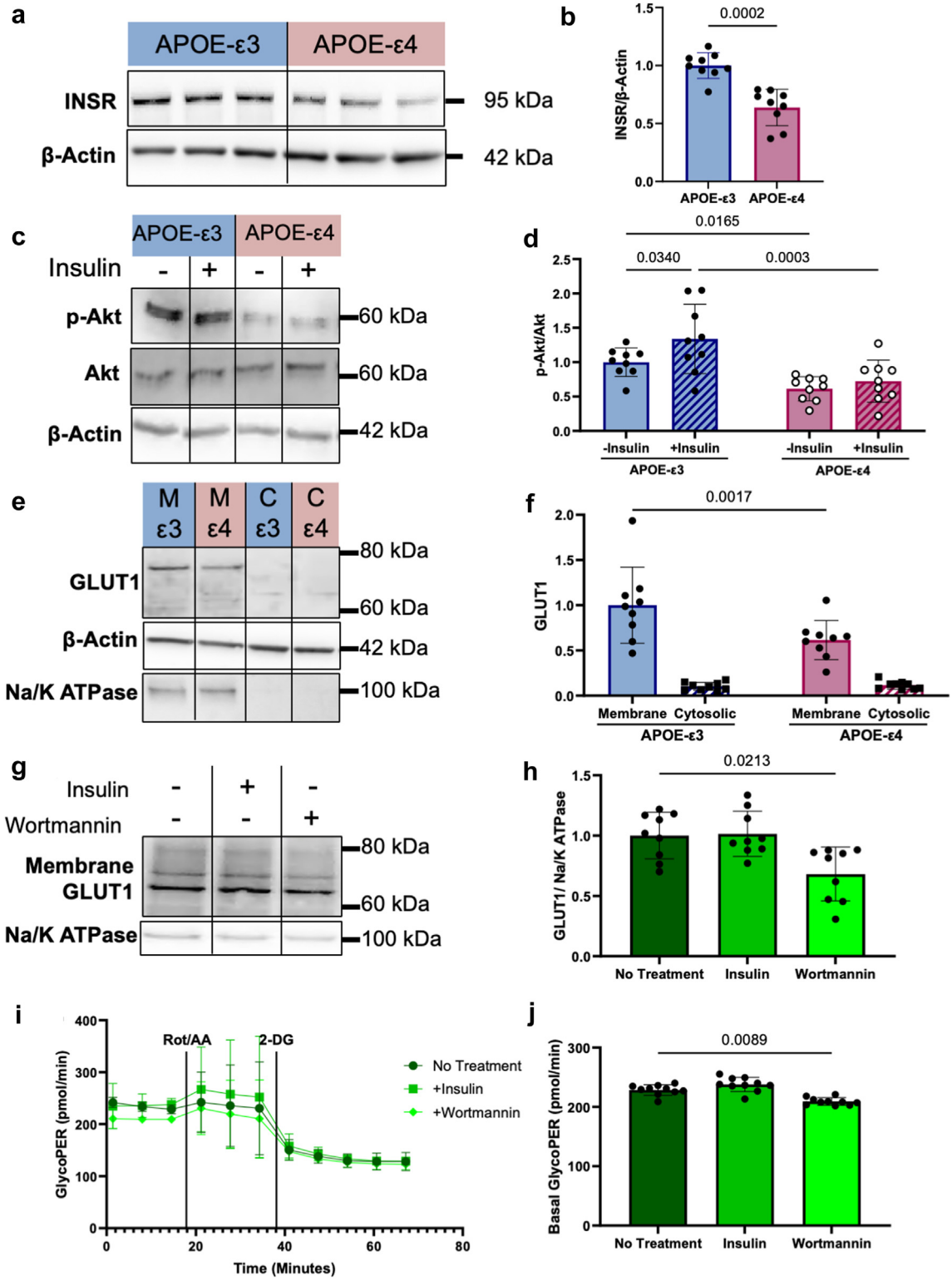

Fig. 5: **Impaired insulin signalling may have contributed to reduced *APOE-ε4* hiBMEC glycolysis. (a, b)** Representative Western blots with quantification of insulin receptor (INSR) in *APOE-ε3* and *-ε4* hiBMEC (n = 9 samples per genotype). **(c, d)** Representative Western blots with quantification of p-Akt and Akt in *APOE-ε3* and *-ε4* hiBMEC treated with 10 μg/mL insulin for 30 min (n = 9 samples per condition). **(e, f)** Representative Western blots with quantification of membrane and cytosolic GLUT1 in *APOE-ε3* and *-ε4* hiBMEC (n = 9 samples per genotype).

AD.[13,48] We therefore examined how serum from exercise trained individuals alters hiBMEC barrier function and metabolism to explore the molecular mechanisms by which exercise benefits brain health. Exercise training has been shown to increase cerebral lactate and AMP-activated protein kinase (AMPK), which in turn increase SIRT1.[19,49,50] Therefore, we hypothesised hiBMEC treated with serum collected post-training would increase SIRT1, barrier function, and glucose metabolism compared to hiBMEC treated with serum collected pre-training.

First, we examined how cardiorespiratory fitness, measured using $\dot{V}_{2peak}$, changed in study participants from the start to the end of the trial (Table 2). Since the $\dot{V}_{2peak}$ change was statistically similar between the low and moderate intensity exercise training groups, the data were combined. Overall, study participants did not have a significant change in $\dot{V}O_{2peak}$ following exercise training.

We then used Western blot to measure SIRT1 levels in *APOE-ε3* and *-ε4* hiBMEC treated with 20% serum collected pre- and post-training (Fig. 6a). Unexpectedly, SIRT1 levels were 71% higher in *APOE-ε4* hiBMEC treated with pre-training serum compared to *APOE-ε3* hiBMEC treated with pre-training serum ($p = 0.0013$ [Repeated Measures Two-Way ANOVA]). While SIRT1 levels in *APOE-ε3* hiBMEC increased by 33% when treated with post-training serum ($p = 0.0043$ [Repeated Measures Two-Way ANOVA]), SIRT1 levels decreased by 22% in *APOE-ε4* hiBMEC treated with post-training serum ($p = 0.0004$ [Repeated Measures Two-Way ANOVA]; Fig. 6b). There was no significant difference in SIRT1 levels between *APOE-ε3* and *-ε4* hiBMEC treated with post-training serum.

Since SIRT1 trends in *APOE-ε3* and *-ε4* hiBMEC were different in the presence of serum compared to those observed in serum-free culture, we next evaluated proteins in the serum that could differentially regulate SIRT1. When we quantified serum SIRT1 via ELISA, there were no significant differences in SIRT1 between *APOE-ε3* and *-ε4* serum samples (Supplementary Fig. S3A). Since *APOE-ε4* proteins can regulate SIRT1 protein,[40,41] we then quantified serum *APOE* via ELISA to see if that could induce the differential SIRT1regulation. *APOE* was also not significantly different between *APOE-ε3* and *-ε4* serum (Supplementary Fig. S3B). Therefore, there are likely other proteins in the serum that regulate SIRT1 in the *APOE-ε3* and *-ε4* hiBMEC.

We next used immunofluorescent imaging with the Junction Analyser Program and TEER to examine if the dimorphic changes in SIRT1 in *APOE-ε3* and *-ε4* hiBMEC with pre-and post-training serum correlated with barrier function changes (Fig. 6c and d). ZO-1 and claudin-5 immunostaining revealed no significant changes in tight junction protein continuity in the *APOE-ε3* or *-ε4* hiBMEC in response to pre- or post-training serum (Fig. 6e and f). There was also no difference in TEER between the *APOE-ε3* and *-ε4* hiBMEC pre- or post-training serum (Fig. 6g).

Post-training serum altered glycolytic enzymes but not glycolysis in *APOE-ε3* and *-ε4* hiBMEC

Since we previously showed changes in glycolytic proteins GLUT1, HK2, and PFKFB3 correlated with changes in SIRT1 in *APOE-ε3* versus *-ε4* hiBMEC, we next examined if these proteins matched the dimorphic changes in SIRT1 in *APOE-ε3* and *-ε4* hiBMEC treated with serum collected pre- and post-exercise training (Fig. 7a). GLUT1 protein levels were similar between *APOE-ε3* and *-ε4* hiBMEC treated with pre-versus post-exercise training serum (Fig. 7b). HK2 protein levels matched SIRT1 changes. HK2 increased by 27% with post-training serum in *APOE-ε3* hiBMEC ($p = 0.0307$ [Repeated Measures Two-Way ANOVA]) but decreased by 15% in *APOE-ε4* hiBMEC treated with post-training serum ($p = 0.0246$ [Repeated Measures Two-Way ANOVA]; Fig. 7c). PFKFB3 protein levels did not change consistently in *APOE-ε3* hiBMEC treated with pre- or post-training serum but decreased by 23% with post-training serum in *APOE-ε4* hiBMEC ($p = 0.0171$ [Repeated Measures Two-Way ANOVA]; Fig. 7d). Other glycolytic enzymes, including GAPDH, LDH, G6PD, and GFAT were not affected by genotype or serum (Supplementary Fig. S3C–G).

YSI and Seahorse Glycolytic Rate Assays were then used to determine if the changes in SIRT1 and glycolytic enzymes resulted in overall changes in glycolysis. Glucose uptake was unchanged between *APOE-ε3* and *-ε4* hiBMEC with pre- or post-training serum (Fig. 7f). Lactate secretion was 5% higher in *APOE-ε4* hiBMEC treated with post-training serum compared to pre-training serum ($p = 0.0218$ [Repeated Measures Two-Way ANOVA], Fig. 7g) but was unchanged in *APOE-ε3* hiBMEC. The Seahorse Glycolytic Rate Assay similarly showed no significant changes in basal glycolysis in *APOE-ε3* or *-ε4* hiBMEC treated with pre- or post-exercise training serum (Fig. 7h).

Serum systemically altered the hiBMEC metabolome, but exercise training did not

Our previous analysis revealed systemic metabolic differences between *APOE-ε3* and *-ε4* hiBMEC. We

(g, h) Representative Western blots with quantification of membrane GLUT1 in hiBMEC treated with 10 μg/mL insulin and 1 μM Wortmannin for 30 min (n = 9 samples per condition). **(i)** Seahorse Glycolytic Rate Assay and **(j)** basal GlycoPER in hiBMEC following treatment with 10 μg/mL and 1 μM Wortmannin for 30 min (n = 10 samples per treatment group). Data were analysed using **(b)** Mann–Whitney test, **(d, f)** Two-way ANOVA with Fishers Least Significant Difference Test, and **(h, j)** Kruskall-Wallis with Dunn's multiple comparison test.

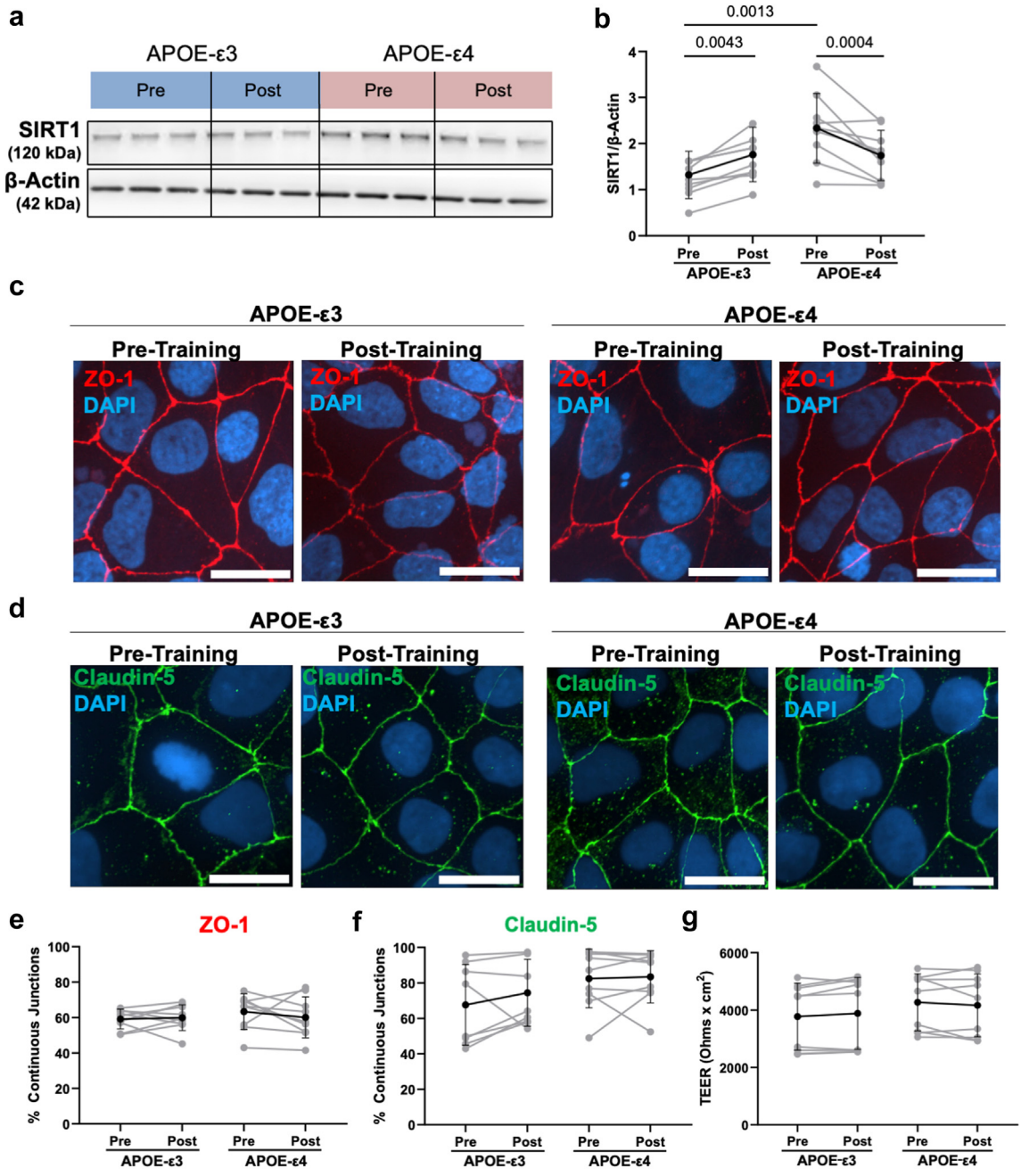

Fig. 6: **SIRT1 increased with post-training serum in *APOE-ε3* hiBMEC and decreased with post-training serum in *APOE-ε4* hiBMEC, but this did not change barrier integrity. (a, b)** Representative Western blot and quantification of SIRT1 in hiBMEC treated with 20% genotype-matched serum for 24 h (n = 9 donors per condition). Representative confocal microscopy images of tight junction proteins **(c)** ZO-1 and **(d)** claudin-5 following serum treatment and **(e, f)** quantified using the junction analyser program (45 cells analysed per donor per treatment group, n = 9 donors per genotype). **(g)** TEER measurements in *APOE-ε3* and *-ε4* hiBMEC following 24 h of treatment with 20% genotype-matched serum. Data analysed using repeated measures two-way ANOVA with Fisher's Least Significant Difference Test.

therefore used LC-MS to examine metabolomic changes in *APOE-ε3* and *-ε4* hiBMEC treated with serum collected pre- and post-exercise training. PLS-DA demonstrated no clear separation of *APOE-ε3* and *-ε4* hiBMEC treated with pre- or post-training serum (Fig. 8a). However, in 3/4 of the *APOE-ε3* hiBMEC samples, the samples shifted rightward shift along PC1 with post-training serum. In contrast, post-training

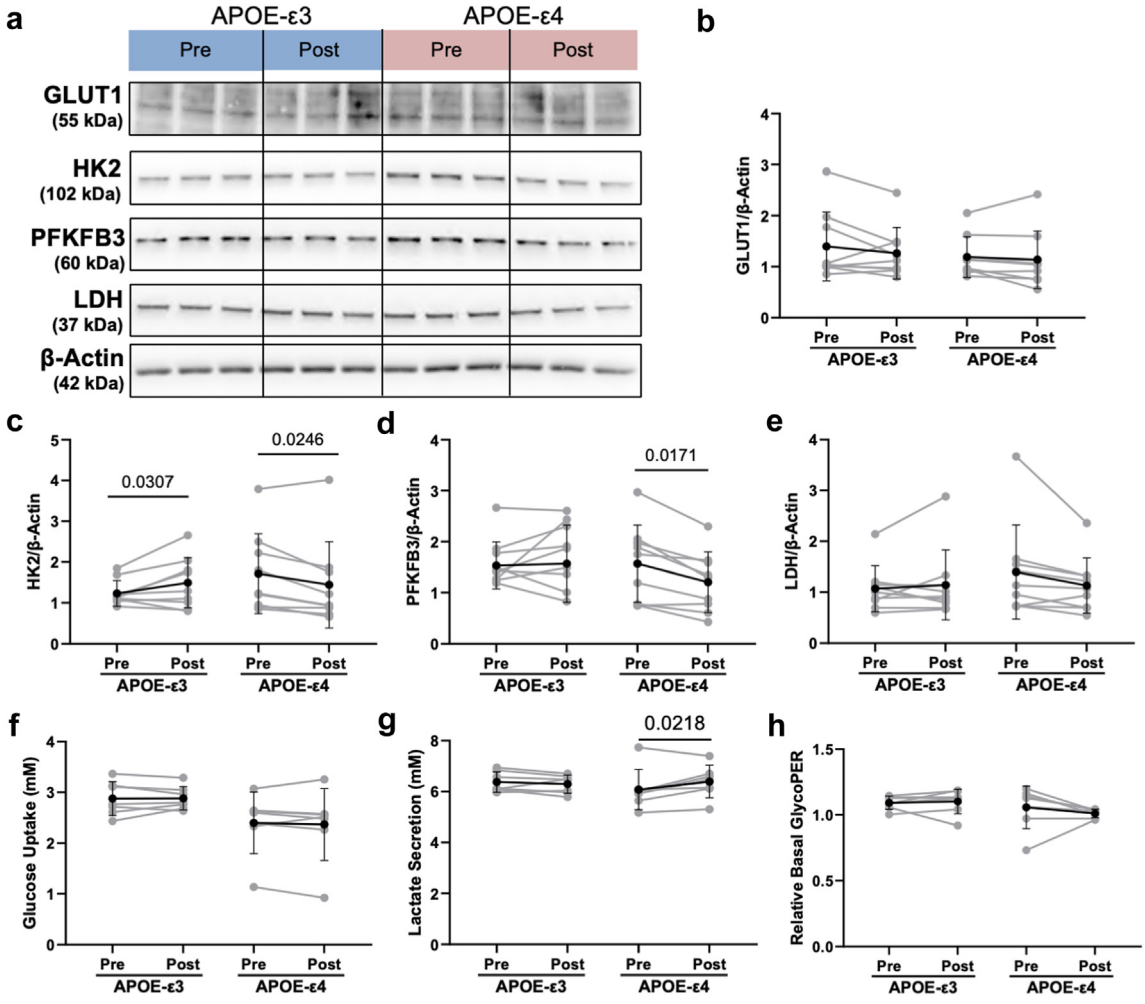

Fig. 7: **Serum from individuals post-training decreased rate limiting glycolytic enzymes HK2 and PFKFB3 in *APOE-ε4* hiBMEC relative to serum collected pre-training. (a)** Representative Western blots with quantification of **(b)** GLUT1, **(c)** HK2, **(d)** PFKFB3, and **(e)** LDH relative to housekeeper β-actin in *APOE-ε3* and *-ε4* hiBMEC following 24 h of treatment with 20% serum from genotype matched individuals pre- and post-exercise training. (n = 9 donors per genotype and condition). Glycolytic measures of **(f)** glucose uptake (YSI), **(g)** lactate secretion (YSI), and **(h)** basal GlycoPER (Seahorse Glycolytic Rate assay) in *APOE-ε3* and *-ε4* hiBMEC following 24 h of treatment with 20% serum from genotype matched individuals pre- and post-exercise training. (n = 9 donors per genotype). Data were analysed using repeated measures two-way ANOVA with Fisher's Least Significant Difference Test.

serum shifted all the *APOE-ε4* hiBMEC samples leftward along PC1. Additionally, 3/4 of the *APOE-ε4* hiBMEC samples treated with post-training serum shifted upwards along PC2 compared to those treated with pre-training serum.

Finally, we analysed how *APOE-ε3* and *-ε4* hiBMEC metabolomes differed with serum addition. For this analysis, samples treated with serum collected pre- and post-training were combined and compared against serum-free *APOE-ε3* and *-ε4* hiBMEC. *APOE-ε3* and *-ε4* hiBMEC did not separate by genotype, as demonstrated by PLS-DA (Fig. 8b). However, serum separated hiBMEC along component 1 (PC1 = 44%). The metabolites that were the largest drivers of this separation are reported in Appendix 6 and include lactate, alanine, pyruvate, (4Z-7Z-10Z-13Z-16Z-19Z)-Docosahexaenoic acid, (9Z)-Octadecenoic acid, fructose 1,6-bisphosphate, and citrate, all of which decreased in hiBMEC treated with serum compared to serum-free hiBMEC culture. The metabolites with the largest contributions to the separation along component 1 largely belonged to glycolysis, fatty acid metabolism, and the TCA cycle.

Discussion

The *APOE-ε4* genotype is one of the largest AD risk factors and is associated with reduced BMEC barrier function and whole brain glucose metabolism. Exercise

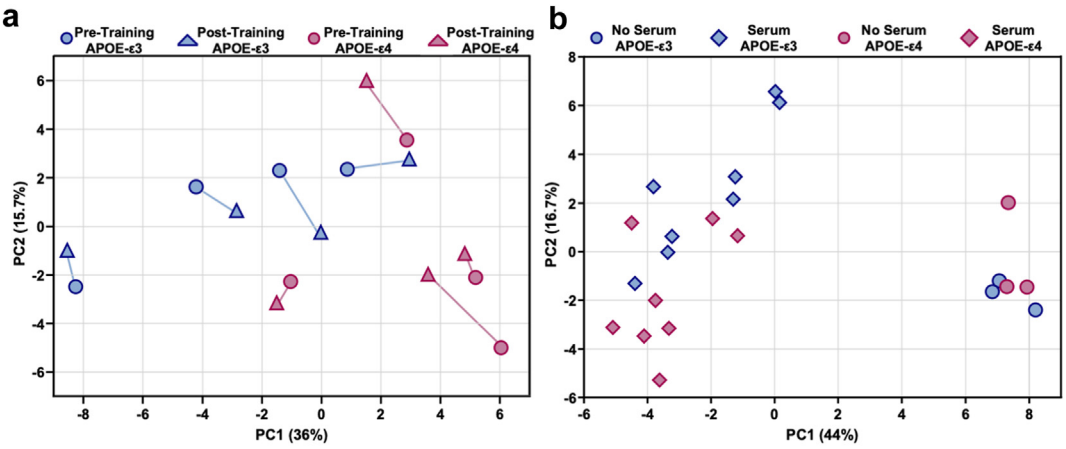

***Fig. 8:* Serum systemically altered the hiBMEC metabolome, but exercise training did not. (a)** PLS-DA of the metabolite labelled fraction of *APOE-ε3* (blue) and *-ε4* (pink) hiBMEC treated for 24 h with 20% serum from genotype-matched individuals pre- (circle) and post- (triangle) exercise training and $^{13}C_6$-glucose. A line connects hiBMEC treated with serum samples from the same donor (n = 4 donors per genotype). **(b)** PLS-DA of the metabolite labelled fraction of *APOE-ε3* (blue) and *-ε4* (pink) hiBMEC treated for 24 h with no serum (circle) or serum (diamond). Serum effects were analysed for combined pre- and post-training serum samples and compared to hiBMEC not treated with serum (n = 8 donors per genotype with serum, n = 3 donors per genotype without serum).

training may counteract AD-related cognitive decline by increasing whole brain glucose metabolism.[14,51] However, there are few, if any, identified mechanisms through which the *APOE* genotype alters barrier function and metabolism, or that investigate how exercise training may support BMEC barrier function and metabolism. Here, we demonstrated that *APOE-ε4* hiBMEC have reduced barrier function and glucose metabolism compared to *APOE-ε3* hiBMEC, and that reduced SIRT1 and insulin signalling may reduce barrier function and glycolysis in *APOE-ε4* hiBMEC. Serum from exercise trained individuals did not significantly alter barrier function or glycolytic rates in hiBMEC but did have dimorphic effects on SIRT1 in *APOE-ε3* and *-ε4* hiBMEC. These findings indicate that the *APOE-ε4* genotype induces BBB breakdown and glucose hypometabolism through SIRT1 and insulin signalling, and these changes cannot be counteracted by serum from exercise-trained individuals alone.

APOE-ε4 hiBMEC had reduced barrier function, as measured through TEER and ZO-1 continuity, relative to the *APOE-ε3* hiBMEC. This agrees with past reports of reduced TEER in BMEC isolated from *APOE-ε4* transgenic mice[9]; increased permeability with reduced ZO-1 and occludin in brain vessels of *APOE-ε4* transgenic mice[10]; and increased BBB permeability in the hippocampus and parahippocampal gyrus of adults who are carriers of the *APOE-ε4* allele.[5] While *APOE-ε4* may reduce barrier function through multiple mechanisms, *APOE-ε4* cells had lower SIRT1. Previous studies have shown that decreasing SIRT1 reduces endothelial barrier integrity. For example, SIRT1 increased ZO-1 in human pulmonary microvascular endothelial cells,[42] BMEC-specific SIRT1 knockout in mice increased BBB permeability,[51] and SIRT1 siRNA knockdown increased mouse[52] and primary human BMEC[43] permeability by decreasing claudin-5. Although the mechanism has not been examined in BMEC, in ovarian cancer cells, SIRT1 deacetylates Krüppel-like factor 4 (KLF4) which promotes claudin-5 transcription.[53] KLF4 can also interact with promotor regions on ZO-1 and occludin to increase their transcription.[54] Therefore, it is possible that the low SIRT1 in *APOE-ε4* hiBMEC increased KLF4 acetylation, which reduced ZO-1 transcription to reduce overall barrier function in *APOE-ε4* hiBMEC.

The *APOE-ε4* genotype is associated with reduced glucose metabolism in transgenic mouse BMEC,[9] astrocytes,[11] and neurons.[55] Here, we showed that these same changes occurred in hiBMEC. Our data suggest that reduced glycolysis may relate to INSR recycling. In neurons, *APOE-ε4* similarly reduced endosomal INSR recycling, which in turn reduced insulin signalling and glycolysis.[47] Neuronal glucose transport is primarily regulated by GLUT3,[56] while hiBMEC glucose transport is primarily regulated by GLUT1. Increased INSR and insulin signalling can increase both GLUT1 and GLUT3 transcription and trafficking of the transporters to the cell membrane.[57–60] Interestingly, in our experiments insulin did not significantly increase membrane GLUT1 or glycolytic rate in hiBMEC. It is therefore possible that the cell membrane is already saturated with GLUT1, and thus GLUT1 translocation cannot increase with additional insulin.

Previous studies demonstrated potential links between glycolysis and barrier function. GLUT1 co-localises with tight junction protein ZO-1 in the

ventromedial hypothalamus, indicating the function of the two proteins may be tightly linked.[61] Reduced GLUT1 also increased vascular permeability in mouse models of AD.[62] Finally, BMEC rely on oxidative phosphorylation for energy when glycolysis is inhibited. Oxidative phosphorylation leads to oxidative stress, which may then damage BBB integrity.[63] Thus, a metabolic shift in *APOE-ε4* BMEC from glycolysis to oxidative phosphorylation could reduce BBB barrier function through oxidative stress. Future studies should examine these mechanisms to identify how reduced glycolysis in *APOE-ε4* hiBMEC reduces barrier function.

$^{13}C_6$-glucose metabolomics revealed systemic metabolomic differences between *APOE-ε3* and *-ε4* hiBMEC. To further delineate metabolic differences, we fit a ^{13}C-MFA model and generated a metabolic flux map. The map unveiled several interesting changes in intracellular metabolism between *APOE-ε3* and *-ε4* hiBMEC, such as reduced GABA production, reversal of α-ketoglutarate-to-glutamate flux, and reversal of the GABA-succinate shuttle flux in *APOE-ε4* hiBMEC. Additionally, *APOE-ε4* hiBMEC have elevated estimated reductive carboxylation and pyruvate carboxylation compared to *APOE-ε3* hiBMEC, both which are associated with lipogenesis.[64,65] In microglia the *APOE-ε4* genotype induces elevated triglyceride and lipid droplet formation, which are neurotoxic.[66] The ^{13}C-MFA predicts that increased fatty acid synthesis may also be occurring in the *APOE-ε4* hiBMEC, which could contribute to neurodegeneration.

Interestingly, SIRT1 is associated with suppression of fatty acid synthase and lipogenesis in hepatocytes through an AMPK-mediated pathway.[67] Lower SIRT1 in *APOE-ε4* hiBMEC may therefore lead to increased activation of fatty acid synthase, which could further increase lipogenic pathways in the *APOE-ε4* hiBMEC. Reductive carboxylation also generates NAD+,[68] which can activate SIRT1 and other sirtuins. This may therefore suggest that reductive carboxylation is used to compensate for reduced SIRT1 levels by increasing activation of available SIRT1 and may help to explain why despite having 27% less SIRT1 protein, there is only 10% less SIRT1 activity in the *APOE-ε4* compared to the *APOE-ε3* hiBMEC.

Serum collected post-6 months of exercise training increased SIRT1 in *APOE-ε3*, but decreased SIRT1 in *APOE-ε4* hiBMEC. A meta-analysis of SIRT1 changes with exercise training demonstrates that acute exercise elevates SIRT1 in skeletal muscle and consistent exercise can elevate circulating SIRT1.[69] Here, we showed that in *APOE-ε3* hiBMEC treated with pre-training serum, SIRT1 levels were significantly lower than in *APOE-ε4* hiBMEC treated with pre-training serum, and that the addition of post-training serum normalised SIRT1 to the same level in *APOE-ε3* and *-ε4* hiBMEC. These data indicate exercise-trained serum may signal for homeostatic control of SIRT1, bringing them back to a general baseline. While SIRT1 levels were higher in *APOE-ε3* hiBMEC compared to *APOE-ε4* hiBMEC without serum treatment, this trend was not shown with serum treatment. Since neither SIRT1 nor *APOE* levels were significantly different between *APOE-ε3* and *-ε4* serum samples, other components of the serum likely regulate intracellular SIRT1 levels.

Since we previously showed SIRT1 regulates barrier function, we hypothesised that post-training serum would increase barrier function in *APOE-ε3* hiBMEC and decrease barrier function in *APOE-ε4* hiBMEC compared to serum collected pre-training. However, we did not see consistent changes in barrier function in response to serum from exercise trained individuals. Aerobic exercise increases cerebral blood flow,[70] and shear stress can increase claudin-5 and ZO-1 levels in human BMEC.[71,72] Thus, it is possible that changes in BBB function relate to increased shear stress rather than serum modifications in response to exercise.

Glycolytic enzyme HK2 followed a similar trajectory as SIRT1 with serum collected post-6 months of exercise training but did not change glycolysis. In leukemia cells, HK2 knockdown increased carbon flux into the PPP and TCA cycle but did not significantly impact glycolysis.[73] Therefore, reduced HK2 in *APOE-ε4* hiBMEC treated with exercise trained serum may alter PPP and TCA pathway activity more than glycolysis. Glycolytic rates are also modulated by many metabolites and proteins outside of the direct glycolytic pathway including ATP bioavailability,[73] so other serum or intracellular factors may also override the changes in HK2 to modulate glycolytic rates.

PLS-DA revealed a clear separation of *APOE-ε3* and *-ε4* hiBMEC metabolites when the cells were cultured in serum-free conditions; however, this separation was no longer apparent when cells were cultured with human serum. Though this could relate to the inherent variability involved when using human serum samples, it is also possible that human serum reduced metabolomic differences between *APOE-ε3* and *-ε4* hiBMEC. Serum decreased intracellular fatty acid synthesis, which may be due to the presence of fatty acids in serum that are not generally present in serum-free cell culture experiments. Overall, the reduction in metabolomic separation between *APOE-ε3* and *-ε4* hiBMEC in the presence of serum reveals that despite intracellular differences, other cells in the body may secrete metabolites, proteins, and fatty acids to naturally regulate genotype-dependent differences in BMEC.

Although the data presented in this study are comprehensive, the study is not without limitations. The study was conducted *in vitro* using an entirely human model, which provides valuable insights into human physiology and pathology. However, *in vivo* animal models incorporate more holistic exercise effects, albeit in a different biological system. A prior *in vivo* analysis

of exercise training in mice supports our results, showing that running increased gene expression associated with vascular integrity more in *APOE-ε3/ε4* than *APOE-ε4/ε4* mice.[74] We used IMR90 iPSC in our *in vitro* model, which we differentiated into BMEC-like cells. IMR90 iPSC are a validated iPSC line homozygous for the *APOE-ε3* genotype,[25] and using one iPSC line enabled us to focus on human serum effects. iPSC-BMEC may also have an underlying epithelial transcriptome that could impact cell response,[75] although we have previously validated that glucose metabolism is similar between hiBMEC and primary BMEC.[23] Finally, this study lacks exercise training-induced physiological cues that are not in the human serum such as altered shear stress.

In conclusion, we demonstrated that the *APOE-ε4* genotype reduces hiBMEC barrier function via SIRT1, and glucose metabolism via insulin signalling. We also showed exercise training may have different impacts on BMEC depending on *APOE* genotype. Future studies should build on these results to examine mechanisms of exercise benefits on brain health, stratified by *APOE* genotype, and develop genotype-dependent exercise recommendations.

Contributors

Conceptualization, C.M.W., B.M., J.C.S., and A.M.C.; Methodology, C.M.W., B.M., G.S.P., G.S.S., J.C.S., and A.M.C., Investigation, C.M.W., B.M., G.S.P., M.K., B.W., C.K., G.S.S.; Formal Analysis, C.M.W., B.M., M.K., B.W., C.K.; Data Curation, C.M.W., B.M., M.K.; Writing- Original Draft, C.M.W. and A.M.C.; Writing- Review & Editing, C.M.W., B.M., G.S.P., J.C.S., and A.M.C.; Visualization, C.M.W. and A.M.C.; Supervision, J.C.S. and A.M.C., Funding Acquisition, J.C.S. and A.M.C. All contributors have read and approved the final version of the manuscript.

Data sharing statement

All data are available in the main text or supplementary materials and can be made available by request to the corresponding author.

Declaration of interests

Authors declare they have no competing interests.

Acknowledgements

The authors would like to thank Sophia Zic, Deborah DiSilvestre, and Ivy Dick for valuable contributions to this research, and the University of Colorado School of Medicine Metabolomics Core for mass spectrometry analysis. AMC acknowledges funding from the Brain Behavior Initiative, NSF CBET 2211966, NIH R01HL165193 and NIH R01HL140239-01. CK and BW acknowledge funding from ASPIRE Program. BM acknowledges funding from Niemann-Pick Disease Foundation and NSF DGE 1632976. JCS acknowledges funding from the Brain Behavior Initiative and R01AG057552. CW acknowledges funding from NSF-GRFP DGE 1840340 and Fischell Fellowship.

Appendix A. Supplementary data

Supplementary data related to this article can be found at https://doi.org/10.1016/j.ebiom.2024.105487.

References

1 Davignon J, Gregg RE, Sing CF. Apolipoprotein E polymorphism and atherosclerosis. *Arteriosclerosis*. 1988;8:1–21. https://doi.org/10.1161/01.ATV.8.1.1.
2 Slooter AJC, Cruts M, Kalmijn S, et al. Risk estimates of dementia by apolipoprotein E genotypes from a population-based incidence study: the rotterdam study. *Arch Neurol*. 1998;55:964. https://doi.org/10.1001/archneur.55.7.964.
3 Fortea J, Pegueroles J, Alcolea D, et al. APOE4 homozygozity represents a distinct genetic form of Alzheimer's disease. *Nat Med*. 2024;30(5):1284–1291. https://doi.org/10.1038/s41591-024-02931-w.
4 Hamer M, Chida Y. Physical activity and risk of neurodegenerative disease: a systematic review of prospective evidence. *Psychol Med*. 2008;39:3–11. https://doi.org/10.1017/S0033291708003681.
5 Montagne A, Nation DA, Sagare AP, et al. APOE4 leads to blood–brain barrier dysfunction predicting cognitive decline. *Nature*. 2020;581:71–76. https://doi.org/10.1038/s41586-020-2247-3.
6 Small GW, Ercoli LM, Silverman DHS, et al. Cerebral metabolic and cognitive decline in persons at genetic risk for Alzheimer's disease. *Proc Natl Acad Sci U S A*. 2000;97:6037–6042. https://doi.org/10.1073/pnas.090106797.
7 Baek MS, Cho H, Lee HS, Lee JH, Ryu YH, Lyoo CH. Effect of APOE ε4 genotype on amyloid-β and tau accumulation in Alzheimer's disease. *Alzheimers Res Ther*. 2020;12:140. https://doi.org/10.1186/s13195-020-00710-6.
8 Nishitsuji K, Hosono T, Nakamura T, Bu G, Michikawa M. Apolipoprotein E regulates the integrity of tight junctions in an isoform-dependent manner in an in vitro blood-brain barrier model. *J Biol Chem*. 2011;286:17536–17542. https://doi.org/10.1074/jbc.M111.225532.
9 Marottoli FM, Trevino TN, Geng X, et al. Autocrine effects of brain endothelial cell-produced human apolipoprotein E on metabolism and inflammation in vitro. *Front Cell Dev Biol*. 2021;9. https://doi.org/10.3389/fcell.2021.668296.
10 Montagne A, Nikolakopoulou AM, Huuskonen MT, et al. APOE4 accelerates advanced-stage vascular and neurodegenerative disorder in old Alzheimer's mice via cyclophilin A independently of amyloid-β. *Nat Aging*. 2021;1:506–520. https://doi.org/10.1038/s43587-021-00073-z.
11 Williams HC, Farmer BC, Piron MA, et al. APOE alters glucose flux through central carbon pathways in astrocytes. *Neurobiol Dis*. 2020;136:104742. https://doi.org/10.1016/j.nbd.2020.104742.
12 Liu J, Min L, Liu R, et al. The effect of exercise on cerebral blood flow and executive function among young adults: a double-blinded randomized controlled trial. *Sci Rep*. 2023;13:8269. https://doi.org/10.1038/s41598-023-33063-9.
13 Smith JC, Nielson KA, Woodard JL, et al. Physical activity reduces hippocampal atrophy in elders at genetic risk for Alzheimer's disease. *Front Aging Neurosci*. 2014;6. https://doi.org/10.3389/fnagi.2014.00061.
14 Dougherty RJ, Schultz SA, Kirby TK, et al. Moderate physical activity is associated with cerebral glucose metabolism in adults at risk for Alzheimer's disease. *J Alzheimers Dis*. 2017;58:1089–1097. https://doi.org/10.3233/JAD-161067.
15 He X, Liu D, Zhang Q, et al. Voluntary exercise promotes glymphatic clearance of amyloid beta and reduces the activation of astrocytes and microglia in aged mice. *Front Mol Neurosci*. 2017;10. https://doi.org/10.3389/fnmol.2017.00144.
16 Baker LD, Frank LL, Foster-Schubert K, et al. Effects of aerobic exercise on mild cognitive impairment. *Arch Neurol*. 2010;67. https://doi.org/10.1001/archneurol.2009.307.
17 Nay K, Smiles WJ, Kaiser J, et al. Molecular mechanisms underlying the beneficial effects of exercise on brain function and neurological disorders. *Int J Mol Sci*. 2021;22:4052. https://doi.org/10.3390/ijms22084052.
18 Lourenco MV, Frozza RL, de Freitas GB, et al. Exercise-linked FNDC5/irisin rescues synaptic plasticity and memory defects in Alzheimer's models. *Nat Med*. 2019;25:165–175. https://doi.org/10.1038/s41591-018-0275-4.
19 El Hayek L, Khalifeh M, Zibara V, et al. Lactate mediates the effects of exercise on learning and memory through SIRT1-dependent activation of hippocampal brain-derived neurotrophic factor (BDNF). *J Neurosci*. 2019;39:1661–1718. https://doi.org/10.1523/JNEUROSCI.1661-18.2019.
20 Moon HY, Becke A, Berron D, et al. Running-induced systemic cathepsin B secretion is associated with memory function. *Cell Metab*. 2016;24:332–340. https://doi.org/10.1016/j.cmet.2016.05.025.
21 Vaynman S, Ying Z, Gomez-Pinilla F. Hippocampal BDNF mediates the efficacy of exercise on synaptic plasticity and cognition. *Eur*

J Neurosci. 2004;20:2580–2590. https://doi.org/10.1111/j.1460-9568.2004.03720.x.
22 Szuhany KL, Bugatti M, Otto MW. A meta-analytic review of the effects of exercise on brain-derived neurotrophic factor. *J Psychiatr Res*. 2015;60:56–64. https://doi.org/10.1016/j.jpsychires.2014.10.003.
23 Weber CM, Moiz B, Zic SM, Alpízar Vargas V, Li A, Clyne AM. Induced pluripotent stem cell-derived cells model brain microvascular endothelial cell glucose metabolism. *Fluids Barriers CNS*. 2022;19:98. https://doi.org/10.1186/s12987-022-00395-z.
24 Percie du Sert N, Hurst V, Ahluwalia A, et al. The ARRIVE guidelines 2.0: updated guidelines for reporting animal research. *PLoS Biol*. 2020;18:e3000410. https://doi.org/10.1371/journal.pbio.3000410.
25 Yu J, Vodyanik MA, Smuga-Otto K, et al. Induced pluripotent stem cell lines derived from human somatic cells. *Science*. 2007;318:1917–1920. https://doi.org/10.1126/science.1151526.
26 Schaffer S, Lam VYM, Ernst IMA, Huebbe P, Rimbach G, Halliwell B. Variability in APOE genotype status in human-derived cell lines: a cause for concern in cell culture studies? *Genes Nutr*. 2014;9:364. https://doi.org/10.1007/s12263-013-0364-4.
27 Schmid B, Prehn KR, Nimsanor N, et al. Generation of a set of isogenic, gene-edited iPSC lines homozygous for all main APOE variants and an APOE knock-out line. *Stem Cell Res*. 2019;34:101349. https://doi.org/10.1016/j.scr.2018.11.010.
28 Neal EH, Marinelli NA, Shi Y, et al. A simplified, fully defined differentiation scheme for producing blood-brain barrier endothelial cells from human iPSCs. *Stem Cell Rep*. 2019;12:1380–1388. https://doi.org/10.1016/j.stemcr.2019.05.008.
29 Neal EH, Katdare KA, Shi Y, Marinelli NA, Hagerla KA, Lippmann ES. Influence of basal media composition on barrier fidelity within human pluripotent stem cell-derived blood-brain barrier models. *J Neurochem*. 2021;159:980–991. https://doi.org/10.1111/jnc.15532.
30 Corbo RM, Scacchi R. Apolipoprotein E (APOE) allele distribution in the world. Is APOE*4 a 'thrifty' allele? *Ann Hum Genet*. 1999;63:301–310. https://doi.org/10.1046/j.1469-1809.1999.6340301.x.
31 Gray KM, Jung JW, Inglut CT, Huang HC, Stroka KM. Quantitatively relating brain endothelial cell-cell junction phenotype to global and local barrier properties under varied culture conditions via the Junction Analyzer Program. *Fluids Barriers CNS*. 2020;17:1–20. https://doi.org/10.1186/s12987-020-0177-y.
32 Nemkov T, Hansen KC, D'Alessandro A. A three-minute method for high-throughput quantitative metabolomics and quantitative tracing experiments of central carbon and nitrogen pathways. *Rapid Commun Mass Spectrom*. 2017;31:663–673. https://doi.org/10.1002/rcm.7834.
33 Nemkov T, D'Alessandro A, Hansen KC. Three-minute method for amino acid analysis by UHPLC and high-resolution quadrupole orbitrap mass spectrometry. *Amino Acids*. 2015;47:2345–2357. https://doi.org/10.1007/s00726-015-2019-9.
34 Millard P, Delépine B, Guionnet M, Heuillet M, Bellvert F, Létisse F. IsoCor: isotope correction for high-resolution MS labeling experiments. *Bioinformatics*. 2019;35:4484–4487. https://doi.org/10.1093/bioinformatics/btz209.
35 Pang Z, Zhou G, Ewald J, et al. Using MetaboAnalyst 5.0 for LC–HRMS spectra processing, multi-omics integration and covariate adjustment of global metabolomics data. *Nat Protoc*. 2022;17:1735–1761. https://doi.org/10.1038/s41596-022-00710-w.
36 Young JD. INCA: a computational platform for isotopically non-stationary metabolic flux analysis. *Bioinformatics*. 2014;30:1333–1335. https://doi.org/10.1093/bioinformatics/btu015.
37 Rahim M, Ragavan M, Deja S, Merritt ME, Burgess SC, Young JD. Inca 2.0: a tool for integrated, dynamic modeling of NMR-and MS-based isotopomer measurements and rigorous metabolic flux analysis. *Metab Eng*. 2022;69:1096–7176. https://doi.org/10.1016/j.ymben.2021.12.009.
38 Moiz B, Garcia J, Basehore S, et al. 13 C metabolic flux analysis indicates endothelial cells Attenuate metabolic perturbations by modulating tca activity. *Metabolites*. 2021;11. https://doi.org/10.3390/metabo11040226.
39 Antoniewicz MR. A guide to 13C metabolic flux analysis for the cancer biologist. *Exp Mol Med*. 2018;50. https://doi.org/10.1038/s12276-018-0060-y.
40 Theendakara V, Peters-Libeu CA, Spilman P, Poksay KS, Bredesen DE, Rao RV. Direct transcriptional effects of apolipoprotein E. *J Neurosci*. 2016;36:685–700. https://doi.org/10.1523/JNEUROSCI.3562-15.2016.
41 Theendakara V, Patent A, Libeu CAP, et al. Neuroprotective sirtuin ratio reversed by ApoE 4. *Proc Natl Acad Sci U S A*. 2013;110:18303–18308. https://doi.org/10.1073/pnas.1314145110.
42 Fu C, Hao S, Xu X, et al. Activation of SIRT1 ameliorates LPS-induced lung injury in mice via decreasing endothelial tight junction permeability. *Acta Pharmacol Sin*. 2019;40:630–641. https://doi.org/10.1038/s41401-018-0045-3.
43 Zhang Y, Cui G, Wang Y, Gong Y, Wang Y. SIRT1 activation alleviates brain microvascular endothelial dysfunction in peroxisomal disorders. *Int J Mol Med*. 2019;44(3):995–1005. https://doi.org/10.3892/ijmm.2019.4250.
44 Chen J, Cao L, Li Z, Li Y. SIRT1 promotes GLUT1 expression and bladder cancer progression via regulation of glucose uptake. *Hum Cell*. 2019;32:193–201. https://doi.org/10.1007/s13577-019-00237-5.
45 Chen Y, Yang H, Chen S, et al. SIRT1 regulated hexokinase-2 promoting glycolysis is involved in hydroquinone-enhanced malignant progression in human lymphoblastoid TK6 cells. *Ecotoxicol Environ Saf*. 2022;241. https://doi.org/10.1016/j.ecoenv.2022.113757.
46 Moiz B, Sriram G, Morss Clyne A. Interpreting metabolic complexity via isotope-assisted metabolic flux analysis Biochemical. *Trends Biochem Sci*. 2023;48. https://doi.org/10.1016/j.tibs.2023.02.001.
47 Zhao N, Liu C-C, Van Ingelgom AJ, et al. Apolipoprotein E4 impairs neuronal insulin signaling by trapping insulin receptor in the endosomes. *Neuron*. 2017;96:115–129.e5. https://doi.org/10.1016/j.neuron.2017.09.003.
48 Zhang S, Zhu L, Peng Y, et al. Long-term running exercise improves cognitive function and promotes microglial glucose metabolism and morphological plasticity in the hippocampus of APP/PS1 mice. *J Neuroinflammation*. 2022;19:34. https://doi.org/10.1186/s12974-022-02401-5.
49 Cantó C, Gerhart-Hines Z, Feige JN, et al. AMPK regulates energy expenditure by modulating NAD+ metabolism and SIRT1 activity. *Nature*. 2009;458:1056–1060. https://doi.org/10.1038/nature07813.
50 Cheng C-K, Shang W, Liu J, et al. Activation of AMPK/miR-181b Axis alleviates endothelial dysfunction and vascular inflammation in diabetic mice. *Antioxidants*. 2022;11:1137. https://doi.org/10.3390/antiox11061137.
51 Gaitán JM, Boots EA, Dougherty RJ, et al. Brain glucose metabolism, cognition, and cardiorespiratory fitness following exercise training in adults at risk for Alzheimer's disease. *Brain Plast*. 2019;5:83–95. https://doi.org/10.3233/BPL-190093.
52 Stamatovic SM, Martinez-Revollar G, Hu A, Choi J, Keep RF, Andjelkovic AV. Decline in Sirtuin-1 expression and activity plays a critical role in blood-brain barrier permeability in aging. *Neurobiol Dis*. 2019;126:105–116. https://doi.org/10.1016/j.nbd.2018.09.006.
53 Zhang X, Chen J, Sun L, Xu Y. SIRT1 deacetylates KLF4 to activate Claudin-5 transcription in ovarian cancer cells. *J Cell Biochem*. 2018;119:2418–2426. https://doi.org/10.1002/jcb.26404.
54 Ma J, Wang P, Liu Y, Zhao L, Li Z, Xue Y. Krüppel-like factor 4 regulates blood-tumor barrier permeability via ZO-1, occludin and claudin-5. *J Cell Physiol*. 2014;229:916–926. https://doi.org/10.1002/jcp.24523.
55 Zhang X, Wu L, Swerdlow RH, Zhao L. Opposing effects of ApoE2 and ApoE4 on glycolytic metabolism in neuronal aging supports a warburg neuroprotective cascade against Alzheimer's disease. *Cells*. 2023;12:410. https://doi.org/10.3390/cells12030410.
56 Nagamatsu S, Kornhauser JM, Burant CF, Seino S, Mayo KE, Bell GI. Glucose transporter expression in brain. cDNA sequence of mouse GLUT3, the brain facilitative glucose transporter isoform, and identification of sites of expression by in situ hybridization. *J Biol Chem*. 1992;267:467–472. https://doi.org/10.1016/S0021-9258(18)48518-3.
57 Taha C, Mitsumoto Y, Liu Z, Skolnik EY, Klip A. The insulin-dependent biosynthesis of GLUT1 and GLUT3 glucose transporters in L6 muscle cells is mediated by distinct pathways. *J Biol Chem*. 1995;270:24678–24681. https://doi.org/10.1074/jbc.270.42.24678.
58 Frazier HN, Ghoweri AO, Anderson KL, et al. Elevating insulin signaling using a constitutively active insulin receptor increases glucose metabolism and expression of GLUT3 in hippocampal neurons. *Front Neurosci*. 2020;14. https://doi.org/10.3389/fnins.2020.00668.

59 Riskin A, Nannegari VH, Mond Y. Acute effectors of GLUT1 glucose transporter subcellular targeting in CIT3 mouse mammary epithelial cells. *Pediatr Res*. 2008;63:56–61. https://doi.org/10.1203/PDR.0b013e31815b440b.

60 Egert S, Nguyen N, Schwaiger M. Myocardial glucose transporter GLUT1: translocation induced by insulin and ischemia. *J Mol Cell Cardiol*. 1999;31:1337–1344. https://doi.org/10.1006/jmcc.1999.0965.

61 Ngarmukos C, Baur EL, Kumagai AK. Co-localization of GLUT1 and GLUT4 in the blood–brain barrier of the rat ventromedial hypothalamus. *Brain Res*. 2001;900:1–8. https://doi.org/10.1016/S0006-8993(01)02184-9.

62 Nguyen HM, Mejia EM, Chang W, et al. Reduction in cardiolipin decreases mitochondrial spare respiratory capacity and increases glucose transport into and across human brain cerebral microvascular endothelial cells. *J Neurochem*. 2016;139:68–80. https://doi.org/10.1111/jnc.13753.

63 Leung SWS, Shi Y. The glycolytic process in endothelial cells and its implications. *Acta Pharmacol Sin*. 2022;43:251–259. https://doi.org/10.1038/s41401-021-00647-y.

64 Metallo CM, Gameiro PA, Bell EL, et al. Reductive glutamine metabolism by IDH1 mediates lipogenesis under hypoxia. *Nature*. 2012;481:380–384. https://doi.org/10.1038/nature10602.

65 Patel MS, Jomain-Baum M, Ballard FJ, Hanson RW. Pathway of carbon flow during fatty acid synthesis from lactate and pyruvate in rat adipose tissue. *J Lipid Res*. 1971;12:179–191. https://doi.org/10.1016/S0022-2275(20)39528-6.

66 Haney MS, Pálovics R, Munson CN, et al. APOE4/4 is linked to damaging lipid droplets in Alzheimer's disease microglia. *Nature*. 2024;628:154–161. https://doi.org/10.1038/s41586-024-07185-7.

67 Hou X, Xu S, Maitland-Toolan KA, et al. SIRT1 regulates hepatocyte lipid metabolism through activating AMP-activated protein kinase. *J Biol Chem*. 2008;283:20015–20026. https://doi.org/10.1074/jbc.M802187200.

68 Cerutti R, Pirinen E, Lamperti C, et al. NAD+-Dependent activation of Sirt1 corrects the phenotype in a mouse model of mitochondrial disease. *Cell Metab*. 2014;19:1042–1049. https://doi.org/10.1016/j.cmet.2014.04.001.

69 Juan CG, Matchett KB, Davison GW. A systematic review and meta-analysis of the SIRT1 response to exercise. *Sci Rep*. 2023;13:14752. https://doi.org/10.1038/s41598-023-38843-x.

70 Kleinloog JPD, Mensink RP, Ivanov D, Adam JJ, Uludağ K, Joris PJ. Aerobic exercise training improves cerebral blood flow and executive function: a randomized, controlled cross-over trial in sedentary older men. *Front Aging Neurosci*. 2019;11. https://doi.org/10.3389/fnagi.2019.00333.

71 Cucullo L, Hossain M, Puvenna V, Marchi N, Janigro D. The role of shear stress in Blood-Brain Barrier endothelial physiology. *BMC Neurosci*. 2011;12. https://doi.org/10.1186/1471-2202-12-40.

72 Ranadewa D, Wu J, Subramanianbalachandar VA, Steward RL. Variable fluid flow regimes alter human brain microvascular endothelial cell–cell junctions and cytoskeletal structure. *Cytoskeleton*. 2021;78:323–334. https://doi.org/10.1002/cm.21687.

73 Bennett NK, Nguyen MK, Darch MA, et al. Defining the ATPome reveals cross-optimization of metabolic pathways. *Nat Commun*. 2020;11:4319. https://doi.org/10.1038/s41467-020-18084-6.

74 Foley KE, Diemler CA, Hewes AA, Garceau DT, Sasner M, Howell GR. *APOE ε4* and exercise interact in a sex-specific manner to modulate dementia risk factors. *Alzheimers Dementia*. 2022;8. https://doi.org/10.1002/trc2.12308.

75 Lu TM, Houghton S, Magdeldin T, et al. Pluripotent stem cell-derived epithelium misidentified as brain microvascular endothelium requires ETS factors to acquire vascular fate. *Proc Natl Acad Sci U S A*. 2021;118. https://doi.org/10.1073/pnas.2016950118.